Available online at www.sciencedirect.com
SCIENCE DIRECT®
Journal of Computational Physics 204 (2005) 193–221
JOURNAL OF COMPUTATIONAL PHYSICS
www.elsevier.com/locate/jcp

The ghost fluid method for compressible gas–water simulation

T.G. Liu [a], B.C. Khoo [b,c,*], C.W. Wang [a]

[a] Institute of High Performance Computing, #01-01 The Capricorn, Singapore Science Park II, Singapore 117528, Singapore
[b] Department of Mechanical Engineering, National University of Singapore, Singapore 119260, Singapore
[c] Singapore-MIT Alliance, 4 Engineering Drive 3, National University of Singapore, Singapore 117576, Singapore

Received 21 January 2004; received in revised form 5 August 2004; accepted 5 October 2004

Abstract

An analysis is carried out for the ghost fluid method (GFM) based algorithm as applied to the gas–water Riemann problems, which can be construed as two single-medium GFM Riemann problems. It is found that the inability to provide correct and consistent Riemann waves in the respective real fluids by these two GFM Riemann problems may lead to inaccurate numerical results. Based on this finding, two conditions are suggested and imposed for the ghost fluid status in order to ensure that correct and consistent Riemann waves are provided in the respective real fluids during the numerical decomposition of the singularity. Using these two conditions to analyse some of the existing GFM-based algorithms such as the original GFM [J. Comput. Phys. 152 (1999) 457], the new version GFM [J. Comput. Phys. 166 (2001) 1; J. Comput. Phys. 175 (2002) 200] and the modified GFM (MGFM) [J. Comput. Phys. 190 (2003) 651], it is found that there are ranges of conditions for each type of solution where either the original GFM or the new version GFM or both are unable to provide correct or consistent Riemann waves in one of the real fluids. Within these ranges, examples can be found such that either the original GFM or the new version GFM or both are unable to provide accurate results. The MGFM is also found to encounter difficulties when applied to nearly cavitating flow. Various examples are presented to demonstrate the conclusions obtained. The MGFM with proposed modification when applied to nearly cavitating flow is then found to be quite robust and can provide relatively reasonable results.

Keywords: Gas–water Riemann problem; Ghost fluid method; Approximate Riemann problem solver; Level-set method; GFM Riemann problem

* Corresponding author. Tel.: +65 874 2889; fax: +65 779 1459.
E-mail addresses: liutg@ihpc.a-star.edu.sg (T.G. Liu), mpekbc@nus.edu.sg (B.C. Khoo).

0021-9991/$ - see front matter © 2004 Elsevier Inc. All rights reserved.
doi:10.1016/j.jcp.2004.10.012

1. Introduction

In general, conservative Eulerian algorithms such as those based on high-resolution conservative schemes like TVD or ENO perform very well when applied to single-medium compressible flows. However, when such an algorithm is employed to solve multi-medium or multi-phase compressible flows, numerical inaccuracies usually occur at the material interfaces due to ''the loss of pressure-invariance property in discretization'' [24]. Various techniques have been developed to try to overcome these difficulties like Larrouturou [17], Karni [15], Abgrall [1], Jenny et al. [14], Cocchi and Saurel [7], and Liu et al. [18,19], to name a few. Among them, some of the resultant algorithms may not maintain the conservative property [7,15,18] in the process of enforcing boundary conditions at the moving material interface so as to better suppress any undesired numerical oscillations. Recent work by van Brummelen and Koren [24] has shown that the numerical oscillation may not be an inherent characteristics of a conservative method when employed for multi-medium flow. In their work, a non-oscillatory conservative method has been developed by defining a compound equation of state for barotropic two-fluid flow to maintain the pressure-invariance property across the interface. The efficiency of this method for flows with more complex equation of state, however, has yet to be verified.

A recently developed method called the ghost fluid method (GFM) by Fedkiw et al. [12] has provided another flexible way to treat the multi-medium flows. The main appealing features of the GFM are its simplicity, easy extension to multi-dimensions and maintenance of a sharp interface without smearing. The GFM makes the interface ''invisible'' during computations and the computations are carried out as for a single-medium manner such that its extension to multi-dimensions becomes fairly straightforward. Since only single-fluid flux formulations are required to make a GFM workable, the GFM is easily employed for two fluids of vastly different types such as a compressible–incompressible or viscous-inviscid two-fluid flow [5]. Simple variants of the original GFM [12] and applications can also be found in [2,16]. Recently, efforts have also been made to develop a conservative GFM as done in [10,21].

On the other hand, it is the manner of treatment of the single medium across the interface in the GFM that may cause numerical inaccuracy when there is a strong shock wave interacting with the interface [20]. This is because the pattern of shock refraction at a material interface and the resultant interfacial status depend highly on material properties on both sides of the interface. In such a situation, the real fluid pressure and velocity at the location of ghost points cannot be just readily assumed to be the ghost fluid pressure and velocity. Reasonable ghost fluid pressure and velocity and thus isobaric value [11] have to be formulated. This has led to the development of a modified GFM (henceforth called MGFM for case of reference) with a predicted ghost fluid status by Liu et al. [20]. Similar work of using an exact Riemann problem solver to construct the ghost fluid state in the whole computational domain can also be found in [3,4].

On applying the GFM [12] to the gas–water flows, special difficulties such as the breakdown of computation [20] can be traced to the sensitivity of pressure to water density change due to the stiff EOS for water. Fedkiw and co-workers [5,13], therefore, proposed an alternative way of constructing the ghost fluid status by using the water medium to determine the interface velocity and the gas medium to provide for the interface pressure. By extrapolating the pressure and velocity, respectively, from the gas and the water to determine the interfacial status, this new version GFM is then (partially) able to take into account the influence of EOS (hereafter, this particular implementation is called the new version GFM for convenience of reference in this work). This has led to a better performance of the latter in applications to gas–water flow [13]. On the other hand, it is found that the latter implementation is not favourable/applicable to the gas–gas flow in contrast to the original GFM [12]. It would certainly be of great interest to provide insight into the fundamental causes. Furthermore, one will find later in Section 4 that the new version GFM is also not sufficient for some situations such as high-speed jet impacting. This may suggest that various procedures such as presented in [2,5,12,13,16] to determine the interface status is not universally effective. The motivation of the present work is, therefore, to analyse the underlying causes via observation that an incorrect or inconsistent Riemann

wave provided by the GFM Riemann problems in the respective real fluids is susceptible to numerical oscillations. We then impose two conditions on the ghost fluid status such that the GFM Riemann problems are able to provide the correct and consistent Riemann waves in the respective real fluids during the numerical decomposition of the singularity. One will find that such conditions can help to identify the ranges of conditions where the GFM based algorithm is unable to provide the correct or consistent Riemann waves in the real fluids. The analysis is carried out primarily using the 1D gas–water Riemann problems.

The remaining text is arranged as follows. In Section 2, the 1D Euler equations are presented together with the EOS for gases and water. Next, the 1D gas–water Riemann problem is discussed and conditions for different types of solution are presented. In Section 3, the same gas–water Riemann problem discussed in Section 2 is divided into two single-medium Riemann problems called the GFM Riemann problems with one-sided ghost fluid status. Analysis is carried out for the two GFM Riemann problems to determine the conditions for the appropriate ghost fluid status so that correct and consistent Riemann waves in the respective real fluids can be provided by the GFM based algorithm. The analysis focuses on the original GFM [12], the new version GFM [5,13] and the MGFM [20] and is carried out for each type of solution. In this section, the MGFM developed in [20] is further modified to cater for nearly cavitating flow. In Section 4, various challenging gas–water Riemann problems are constructed based on the analysis and conditions developed in Section 3. A brief conclusion is given in Section 5.

2. The gas–water Riemann problem

2.1. 1D Euler equation

The 1D Euler equations of an initial-value Riemann problem can be written as

$$\frac{\partial U}{\partial t}+\frac{\partial F(U)}{\partial x}=0, \quad U|_{t=0}=\begin{cases} U_{\mathrm{l}}, & x<x_0, \\ U_{\mathrm{r}}, & x>x_0, \end{cases} \tag{2.1}$$

for an inviscid, non-heat-conducting compressible flow, where $U=[\rho,\rho u,E]^{\mathrm{T}}$, $F(U)=[\rho u,\rho u^2+p,(E+p)u]^{\mathrm{T}}$, ρ is the density, u is the velocity, p is the pressure and E is the total energy. U_{l} and U_{r} are two constant states separated by the gas–water interface located at x_0 Hereafter, the subscripts "l" and "r" indicate the flow state on the left and right media, respectively, which can be either a gas or water medium. The total energy is given as

$$E=\rho e+\rho u^2/2, \tag{2.2}$$

where e is the specific internal energy per mass. For closure of system, the EOS is required. The γ-law used for gases is

$$\rho e=p/(\gamma-1). \tag{2.3}$$

The Tait EOS employed for the water medium has the form [9],

$$p=B[\rho/\rho_0]^N-B+A, \tag{2.4}$$

where $N=7.0$, $A=1.0\mathrm{E}5$ Pa, $B=3.0\mathrm{E}8$ Pa and $\rho_0=1000.0$ kg/m^3 in this work. For the water flow, cavitation can occur when pressure is lower than a critical level. With the appearance of cavitation, flow phase transition occurs. A proper EOS in the cavitation region has yet to be successfully developed, which is universally accepted. As such, also, this is not within the scope of the present work.

The Tait EOS is independent of entropy and hence strictly the energy equation is not required for solving the compressible water flow. To facilitate programming, however, an expression for the internal energy associated with the Tait EOS can be developed as in [6,12,18]

$$\rho e = (p + N\bar{B})/(N-1), \tag{2.5}$$

where $\bar{B} = B - A$. In this way, one can directly apply the numerical solvers developed for the compressible gas flow to the water medium.

2.2. Solution of the gas–water Riemann problem

In the absence of cavitation, the solution types of a gas–water Riemann problem are very similar to those of a single gas Riemann problem and have been studied by Tang and Huang [22]. The solution in general consists of four constant regions connected with three centred Riemann waves – a shock wave, a rarefaction wave and a contact discontinuity. For ease of discussion and reference, we shall categorise the solution into three types: Category I – a rarefaction wave and a shock wave connected by a contact discontinuity; Category II – double shock waves connected by a contact discontinuity; Category III – double rarefaction waves connected by a contact discontinuity. We are interested in the conditions that give rise to solution belonging to Category I, II or III. Such conditions will serve as guidelines for analysing the GFM in Section 3. We shall further use a symbol like ${}^{\mathrm{G}}_{\mathrm{R}}|^{\mathrm{W}}_{\mathrm{S}}$ to denote a particular type of the solution; the upper two letters stand for the media on the respective left and right sides of the interface while the lower two letters specify the non-linear Riemann waves in the associated media. The symbol, ${}^{\mathrm{G}}_{\mathrm{R}}|^{\mathrm{W}}_{\mathrm{S}}$, means that the gas (denoted by "G") and the water (denoted by "W") are located in the respective left and right sides of the interface and that a left rarefaction wave (denoted by "R") and a right shock wave (denoted by "S") are generated in the respective gas and water media after the diaphragm is removed. If "R" or "S" is replaced by "−", it means that there is no Riemann wave in that medium under special initial conditions. The discussions and conclusions to be reached below are obtained under the assumption that pressure is increased across a shock front while it is decreased through a rarefaction wave fan. The detailed derivation is omitted, as the analysis is very similar to that done for a perfect gas Riemann problem and available in [23]. We shall further assume that the gas is located on the left while the water is on the right for the following analysis.

For Category I, we have Conclusions 2.1 and 2.2 depending on the initial flow status on the left and right sides of the interface.

Conclusion 2.1. *If the initial status of* U_{l} *and* U_{r} *satisfies the conditions of*

$$p_{\mathrm{l}} > p_{\mathrm{r}} \quad \textit{and} \quad \frac{2c_{\mathrm{l}}}{\gamma-1}\left[\left(\frac{p_{\mathrm{r}}}{p_{\mathrm{l}}}\right)^{\frac{\gamma-1}{2\gamma}} - 1\right] < u_{\mathrm{l}} - u_{\mathrm{r}} < \sqrt{\frac{\bar{p}_{\mathrm{r}}}{\rho_{\mathrm{r}}}}\sqrt{\frac{\bar{p}_{\mathrm{l}}}{\bar{p}_{\mathrm{r}}} - 1}\sqrt{1 - \left(\frac{\bar{p}_{\mathrm{l}}}{\bar{p}_{\mathrm{r}}}\right)^{-1/N}}, \tag{2.6}$$

then the solution type is ${}^{\mathrm{G}}_{\mathrm{R}}|^{\mathrm{W}}_{\mathrm{S}}$.

Here, $\bar{p} = p + \bar{B}$ and c is the speed of sound for the gas. There are two special cases, ${}^{\mathrm{G}}_{-}|^{\mathrm{W}}_{\mathrm{S}}$ and ${}^{\mathrm{G}}_{\mathrm{R}}|^{\mathrm{W}}_{-}$. It can be deduced from (2.6) that

Conclusions 2.1a & 2.1b. *If the initial status of* U_{l} and $\mathrm{U_r}$ satisfies the conditions of

$$p_{\mathrm{l}} > p_{\mathrm{r}} \quad \textit{and} \quad u_{\mathrm{l}} - u_{\mathrm{r}} = \sqrt{\frac{\bar{p}_{\mathrm{r}}}{\rho_{\mathrm{r}}}}\sqrt{\frac{\bar{p}_{\mathrm{l}}}{\bar{p}_{\mathrm{r}}} - 1}\sqrt{1 - \left(\frac{\bar{p}_{\mathrm{l}}}{\bar{p}_{\mathrm{r}}}\right)^{-1/N}} > 0, \tag{2.6a}$$

then the solution type is ${}^{\mathrm{G}}_{-}|^{\mathrm{W}}_{\mathrm{S}}$, *while if the initial status of* U_{l} *and* U_{r} *satisfies the conditions of*

$$p_{\mathrm{l}} > p_{\mathrm{r}} \quad \textit{and} \quad u_{\mathrm{l}} - u_{\mathrm{r}} = \frac{2c_{\mathrm{l}}}{\gamma-1}\left[\left(\frac{p_{\mathrm{r}}}{p_{\mathrm{l}}}\right)^{\frac{\gamma-1}{2\gamma}} - 1\right] < 0, \tag{2.6b}$$

then the solution type is ${}^{\mathrm{G}}_{\mathrm{R}}|^{\mathrm{W}}_{-}$. The latter (2.6b) pertains to Conclusion 2.1b.

Conclusion 2.2. *If the initial status of U_l and U_r satisfies the conditions of*

$$p_l < p_r \quad \text{and} \quad \frac{2\bar{c}_r}{N-1}\left[\left(\frac{\bar{p}_l}{\bar{p}_r}\right)^{\frac{N-1}{2N}} - 1\right] < u_l - u_r < \sqrt{\frac{\beta p_l}{\rho_l}}\frac{p_r/p_l - 1}{\sqrt{1+\tau p_r/p_l}}, \tag{2.7}$$

then the solution type is $\overset{G}{S}|\overset{W}{R}$.

Here $\beta = 2/(\gamma - 1)$, $\tau = (\gamma + 1)/(\gamma - 1)$ and $\bar{c}$ represents the sound speed of water. The two special cases are $\overset{G}{-}|\overset{W}{R}$ and $\overset{G}{S}|\overset{W}{-}$. For these two special cases, we have the following conclusions:

Conclusions 2.2a & 2.2b. *If the initial status of U_l and U_r satisfies the conditions of*

$$p_l < p_r \quad \text{and} \quad u_l - u_r = \sqrt{\frac{\beta p_l}{\rho_l}}\frac{p_r/p_l - 1}{\sqrt{1+\tau p_r/p_l}} > 0, \tag{2.7a}$$

then the solution type is $\overset{G}{S}|\overset{W}{-}$, *while if the initial status of U_l and U_r satisfies the conditions of*

$$p_l < p_r \quad \text{and} \quad u_l - u_r = \frac{2\bar{c}_r}{N-1}\left[\left(\frac{\bar{p}_l}{\bar{p}_r}\right)^{\frac{N-1}{2N}} - 1\right] < 0, \tag{2.7b}$$

then the solution type is $\overset{G}{-}|\overset{W}{R}$. The latter (2.7b) pertains to Conclusion 2.2b.

For Category II, we have Conclusion 2.3:

Conclusion 2.3. *If the initial status of U_l and U_r satisfies the conditions of*

$$p_l > p_r \quad \text{and} \quad u_l - u_r > \sqrt{\frac{\bar{p}_r}{\rho_r}}\sqrt{\frac{\bar{p}_l}{\bar{p}_r} - 1}\sqrt{1 - \left(\frac{\bar{p}_l}{\bar{p}_r}\right)^{-1/N}} > 0, \tag{2.8a}$$

or conditions of

$$p_l < p_r \quad \text{and} \quad u_l - u_r > \sqrt{\frac{\beta p_l}{\rho_l}}\frac{p_r/p_l - 1}{\sqrt{1+\tau p_r/p_l}} > 0, \tag{2.8b}$$

then the solution type is $\overset{G}{S}|\overset{W}{S}$.

For Category III, we have Conclusion 2.4:

Conclusion 2.4. *If the initial status of U_l and U_r satisfies the conditions of*

$$p_l > p_r \quad \text{and} \quad -\frac{2c_l}{\gamma-1} - \frac{2\bar{c}_r k_{cr}}{N-1} < u_l - u_r < \frac{2c_l}{\gamma-1}\left[\left(\frac{p_r}{p_l}\right)^{\frac{\gamma-1}{2\gamma}} - 1\right] < 0, \tag{2.9a}$$

or conditions of

$$p_l < p_r \quad \text{and} \quad -\frac{2c_l}{\gamma-1} - \frac{2\bar{c}_r k_{cr}}{N-1} < u_l - u_r < \frac{2\bar{c}_r}{N-1}\left[\left(\frac{\bar{p}_l}{\bar{p}_r}\right)^{\frac{N-1}{2N}} - 1\right] < 0, \tag{2.9b}$$

then the solution type is $\overset{G}{R}|\overset{W}{R}$.

Here $k_{cr} = [1 - (B/\bar{p}_r)^{\frac{N-1}{2N}}]$. It should be noted that for Conclusion 2.4, the water cavitation pressure (i.e. the critical pressure) is assumed to be zero. Under this assumption, we have

Conclusion 2.4a. *If the initial status of U_l and U_r satisfies the conditions of*

$$u_l - u_r < -\frac{2c_l}{\gamma - 1} - \frac{2\bar{c}_r k_{cr}}{N - 1}, \tag{2.10}$$

then cavitation occurs [22].

From Conclusions 2.1–2.4, one can easily deduce the following.

Conclusion 2.5. *If initially $p_l = p_r$ is true, then the solution type is $\overset{G}{-}|\overset{W}{-}$, $\overset{G}{R}|\overset{W}{R}$ or $\overset{G}{S}|\overset{W}{S}$ corresponding to $u_l = u_r$, $u_l < u_r$ or $u_l > u_r$, respectively. If initially $u_l = u_r$ is true, the solution type belongs to Category I with a rarefaction wave and a shock wave in the respective high and low pressure regions.*

Conclusion 2.6.

If the solution type is $\overset{G}{R}|\overset{W}{S}$, then $u_I > \max(u_l, u_r)$ and $p_r < p_I < p_l$.
If the solution type is $\overset{G}{S}|\overset{W}{R}$, then $u_I < \min(u_l, u_r)$ and $p_l < p_I < p_r$.
If the solution type is $\overset{G}{S}|\overset{W}{S}$, then $u_r < u_I < u_l$ and $p_I > \max(p_l, p_r)$.
If the solution type is $\overset{G}{R}|\overset{W}{R}$, then $u_l < u_I < u_r$ and $p_I < \min(p_l, p_r)$.

Conclusions 2.5 and 2.6 are also true for single medium (gas–gas or water–water) Riemann problems for each type of solution. (Such Conclusions are useful when we consider the ghost state for the GFM Riemann problems in Section 3.)

Here u_I and p_I are the interfacial velocity and pressure after the decomposition of the initial singularity. It can be shown that the conditions indicated in the respective Conclusions 2.1–2.4 are also necessary. (If the water medium is assumed to be located on the left and the gas is on the right, similar Conclusions as 2.1–2.6 can be derived for the conditions applicable and leading to the respective types of solution.) The conclusions obtained in this section are summarised in Table 1 for convenience of reference in Section 3.

As one of the GFM Riemann problems is a single gas Riemann problem and the other is a single liquid Riemann problem, similar Conclusions of 2.1–2.4 for the single gas throughout Riemann problem or single water throughout Riemann problem will be applied in Section 3. Below are summarised the equivalent Conclusions of 2.1–2.4 for the single gas and single water Riemann problems in Tables 2 and 3, respectively; these serve to facilitate the discussion in Section 3.

One may have noted that the conditions for providing each type of solution depend not only on the initial flow dynamic parameters (pressure and velocity) but also non-linearly on the material properties (EOS) of both fluids. This implies that the influence from the material properties strictly have to be taken into account during the numerical decomposition of the singularity at the interface. In other words, the ghost fluid status generally has to take into account such influence in order that a GFM based algorithm can provide or enable accurate calculations.

3. The GFM on the gas–water Riemann problem

Physically, once the diaphragm separating the gas and the water is removed, the interface recovers to its normal motion instantly, where the initial pressure and velocity discontinuities disappear simultaneously. (Here, the normal motion means that the pressure and normal velocity are continuous across the interface.) However, it takes a few or as many computational steps as necessary to reach this state numerically. It is within the first few steps that numerical errors can cause inaccuracy or breakdown of computation. In the first few steps, a GFM based algorithm essentially consists of solving two separate Riemann problems in the two respective (single) medium with one-sided ghost fluid. One is in the gas medium with the initial conditions of

Table 1
Summary of Conclusions 2.1–2.6 for gas–water Riemann problems

Conclusion	Solution type	Conditions	Equation
Category I			
2.1	$\begin{smallmatrix}\mathrm{G}\\ \mathrm{R}\end{smallmatrix}\big\|\begin{smallmatrix}\mathrm{W}\\ \mathrm{S}\end{smallmatrix}$	$p_l > p_r,\quad \frac{2c_l}{\gamma-1}\left[\left(\frac{p_r}{p_l}\right)^{\frac{\gamma-1}{2\gamma}}-1\right] < u_l-u_r < \sqrt{\frac{\bar{p}_r}{\rho_r}}\sqrt{\frac{\bar{p}_l}{\bar{p}_r}-1}\sqrt{1-\left(\frac{\bar{p}_l}{\bar{p}_r}\right)^{-1/N}}$	(2.6)
2.1a	$\begin{smallmatrix}\mathrm{G}\\ -\end{smallmatrix}\big\|\begin{smallmatrix}\mathrm{W}\\ \mathrm{S}\end{smallmatrix}$	$p_l > p_r,\quad u_l-u_r = \sqrt{\frac{\bar{p}_r}{\rho_r}}\sqrt{\frac{\bar{p}_l}{\bar{p}_r}-1}\sqrt{1-\left(\frac{\bar{p}_l}{\bar{p}_r}\right)^{-1/N}} > 0$	(2.6a)
2.1b	$\begin{smallmatrix}\mathrm{G}\\ \mathrm{R}\end{smallmatrix}\big\|\begin{smallmatrix}\mathrm{W}\\ \mathrm{S}\end{smallmatrix}$	$p_l > p_r,\quad u_l-u_r = \frac{2\bar{c}_l}{N-1}\left[\left(\frac{\bar{p}_r}{\bar{p}_l}\right)^{\frac{N-1}{2N}}-1\right] < 0$	(2.6b)
2.2	$\begin{smallmatrix}\mathrm{G}\\ \mathrm{S}\end{smallmatrix}\big\|\begin{smallmatrix}\mathrm{W}\\ \mathrm{R}\end{smallmatrix}$	$p_l < p_r,\quad \frac{2\bar{c}_r}{N-1}\left[\left(\frac{\bar{p}_l}{\bar{p}_r}\right)^{\frac{N-1}{2N}}-1\right] < u_l-u_r < \sqrt{\frac{\beta p_l}{\rho_l}}\frac{p_r/p_l-1}{\sqrt{1+\tau p_r/p_l}}$	(2.7)
2.2a	$\begin{smallmatrix}\mathrm{G}\\ \mathrm{S}\end{smallmatrix}\big\|\begin{smallmatrix}\mathrm{W}\\ -\end{smallmatrix}$	$p_l < p_r,\quad u_l-u_r = \sqrt{\frac{\beta p_l}{\rho_l}}\frac{p_r/p_l-1}{\sqrt{1+\tau p_r/p_l}} > 0$	(2.7a)
2.2b	$\begin{smallmatrix}\mathrm{G}\\ -\end{smallmatrix}\big\|\begin{smallmatrix}\mathrm{W}\\ \mathrm{R}\end{smallmatrix}$	$p_l < p_r,\quad u_l-u_r = \frac{2\bar{c}_r}{N-1}\left[\left(\frac{\bar{p}_l}{\bar{p}_r}\right)^{\frac{N-1}{2N}}-1\right] < 0$	(2.7b)
Category II			
2.3	$\begin{smallmatrix}\mathrm{G}\\ \mathrm{S}\end{smallmatrix}\big\|\begin{smallmatrix}\mathrm{W}\\ \mathrm{S}\end{smallmatrix}$	$p_l > p_r,\quad u_l-u_r > \sqrt{\frac{\bar{p}_r}{\rho_r}}\sqrt{\frac{\bar{p}_l}{\bar{p}_r}-1}\sqrt{1-\left(\frac{\bar{p}_l}{\bar{p}_r}\right)^{-1/N}} > 0$	(2.8a)
		$p_l < p_r,\quad u_l-u_r > \sqrt{\frac{\beta p_l}{\rho_l}}\frac{p_r/p_l-1}{\sqrt{1+\tau p_r/p_l}} > 0$	(2.8b)
Category III			
2.4	$\begin{smallmatrix}\mathrm{G}\\ \mathrm{R}\end{smallmatrix}\big\|\begin{smallmatrix}\mathrm{W}\\ \mathrm{R}\end{smallmatrix}$	$p_l > p_r,\quad -\frac{2c_l}{\gamma-1}-\frac{2\bar{c}_r k_{cr}}{N-1} < u_l-u_r < \frac{2c_l}{\gamma-1}\left[\left(\frac{p_r}{p_l}\right)^{\frac{\gamma-1}{2\gamma}}-1\right] < 0$	(2.9a)
		$p_l < p_r,\quad -\frac{2c_l}{\gamma-1}-\frac{2\bar{c}_r k_{cr}}{N-1} < u_l-u_r < \frac{2\bar{c}_r}{N-1}\left[\left(\frac{\bar{p}_l}{\bar{p}_r}\right)^{\frac{N-1}{2N}}-1\right] < 0$	(2.9b)
2.4a	$\begin{smallmatrix}\mathrm{G}\\ \mathrm{R}\end{smallmatrix}\big\|\begin{smallmatrix}\mathrm{W}\\ \mathrm{R}\end{smallmatrix}$	$u_l-u_r < -\frac{2c_l}{\gamma-1}-\frac{2\bar{c}_r k_{cr}}{N-1}$	(2.10)
Initial constant pressure or velocity cases			
2.5	$\begin{smallmatrix}\mathrm{G}\\ -\end{smallmatrix}\big\|\begin{smallmatrix}\mathrm{W}\\ -\end{smallmatrix}$	$p_l = p_r,\ u_l = u_r$	
	$\begin{smallmatrix}\mathrm{G}\\ \mathrm{R}\end{smallmatrix}\big\|\begin{smallmatrix}\mathrm{W}\\ \mathrm{R}\end{smallmatrix}$	$p_l = p_r,\ u_l < u_r$	
	$\begin{smallmatrix}\mathrm{G}\\ \mathrm{S}\end{smallmatrix}\big\|\begin{smallmatrix}\mathrm{W}\\ \mathrm{S}\end{smallmatrix}$	$p_l = p_r,\ u_l > u_r$	
	$\begin{smallmatrix}\mathrm{G}\\ \mathrm{R}\end{smallmatrix}\big\|\begin{smallmatrix}\mathrm{W}\\ \mathrm{S}\end{smallmatrix}$	$p_l > p_r,\ u_l = u_r$	
	$\begin{smallmatrix}\mathrm{G}\\ \mathrm{S}\end{smallmatrix}\big\|\begin{smallmatrix}\mathrm{W}\\ \mathrm{R}\end{smallmatrix}$	$p_l < p_r,\ u_l = u_r$	
Interfacial status			
2.6	$\begin{smallmatrix}\mathrm{G}\\ \mathrm{R}\end{smallmatrix}\big\|\begin{smallmatrix}\mathrm{W}\\ \mathrm{S}\end{smallmatrix}$	$u_I > \max(u_l,u_r),\ p_r < p_I < p_l$	
	$\begin{smallmatrix}\mathrm{G}\\ \mathrm{S}\end{smallmatrix}\big\|\begin{smallmatrix}\mathrm{W}\\ \mathrm{R}\end{smallmatrix}$	$u_I < \min(u_l,u_r),\ p_l < p_I < p_r$	
	$\begin{smallmatrix}\mathrm{G}\\ \mathrm{R}\end{smallmatrix}\big\|\begin{smallmatrix}\mathrm{W}\\ \mathrm{R}\end{smallmatrix}$	$u_l < u_I < u_r,\ p_I < \min(p_l,p_r)$	
	$\begin{smallmatrix}\mathrm{G}\\ \mathrm{S}\end{smallmatrix}\big\|\begin{smallmatrix}\mathrm{W}\\ \mathrm{S}\end{smallmatrix}$	$u_r < u_I < u_l,\ p_I > \max(p_l,p_r)$	

$$U|_{t=0} = \begin{cases} U_l, & x < x_0, \\ U_r^*, & x > x_0 \end{cases} \tag{3.1a}$$

and it solves from the grid point 1 on the left end to the ghost point(s). The other is in the water with the initial conditions of

$$U|_{t=0} = \begin{cases} U_l^*, & x < x_0, \\ U_r, & x > x_0 \end{cases}, \tag{3.1b}$$

and it solves from the ghost point(s) to the end point on the right. Here (and henceforth), "*" indicates the ghost fluid (status). We call these two single-medium Riemann problems, (3.1a) and (3.1b), the GFM Riemann problems; this is to distinguish it from the Riemann problem (2.1) called the original Riemann problem.

In (3.1a) and (3.1b), the ghost fluid status is not specified. It seems that one has the freedom of choice to construct the ghost fluid status such that the premise of keeping continuity of pressure and normal velocity

Table 2
Summary of equivalent Conclusions 2.1–2.4 for gas–gas Riemann problems (and applicable for G–G* GFM Riemann problem in Section 3)

Conclusion	Solution type	Conditions	Equation
Category I			
2.1-gas	$\overset{G}{R}\vert\overset{G}{S}$	$p_l > p_r,\quad \frac{2c_l}{\gamma-1}\left[\left(\frac{p_r}{p_l}\right)^{\frac{\gamma-1}{2\gamma}}-1\right] < u_l-u_r < \sqrt{\frac{\beta p_r}{\rho_r}}\frac{p_l/p_r-1}{\sqrt{1+\tau p_l/p_r}}$	(2.6-gas)
2.1a-gas	$\overset{G}{-}\vert\overset{G}{S}$	$p_l > p_r,\quad u_l-u_r = \sqrt{\frac{\beta p_r}{\rho_r}}\frac{p_l/p_r-1}{\sqrt{1+\tau p_l/p_r}} > 0$	(2.6a-gas)
2.1b-gas	$\overset{G}{R}\vert\overset{G}{-}$	$p_l > p_r,\quad u_l-u_r = \frac{2c_l}{\gamma-1}\left[\left(\frac{p_r}{p_l}\right)^{\frac{\gamma-1}{2\gamma}}-1\right] < 0$	(2.6b-gas)
2.2-gas	$\overset{G}{S}\vert\overset{G}{R}$	$p_l < p_r,\quad \frac{2c_r}{\gamma-1}\left[\left(\frac{p_l}{p_r}\right)^{\frac{\gamma-1}{2\gamma}}-1\right] < u_l-u_r < \sqrt{\frac{\beta p_l}{\rho_l}}\frac{p_r/p_l-1}{\sqrt{1+\tau p_r/p_l}}$	(2.7-gas)
2.2a-gas	$\overset{G}{S}\vert\overset{G}{-}$	$p_l < p_r,\quad u_l-u_r = \sqrt{\frac{\beta p_l}{\rho_l}}\frac{p_r/p_l-1}{\sqrt{1+\tau p_r/p_l}} > 0$	(2.7a-gas)
2.2b-gas	$\overset{G}{-}\vert\overset{G}{R}$	$p_l < p_r,\quad u_l-u_r = \frac{2c_r}{\gamma-1}\left[\left(\frac{p_l}{p_r}\right)^{\frac{\gamma-1}{2\gamma}}-1\right] < 0$	(2.7b-gas)
Category II			
2.3-gas	$\overset{G}{S}\vert\overset{G}{S}$	$p_l > p_r,\quad u_l-u_r > \sqrt{\frac{\beta p_r}{\rho_r}}\frac{p_l/p_r-1}{\sqrt{1+\tau p_l/p_r}} > 0$	(2.8a-gas)
		$p_l < p_r,\quad u_l-u_r > \sqrt{\frac{\beta p_l}{\rho_l}}\frac{p_r/p_l-1}{\sqrt{1+\tau p_r/p_l}} > 0$	(2.8b-gas)
Category III			
2.4-gas	$\overset{G}{R}\vert\overset{G}{R}$	$p_l > p_r,\quad -\frac{2c_l}{\gamma-1}-\frac{2c_r}{\gamma-1} < u_l-u_r < \frac{2c_l}{\gamma-1}\left[\left(\frac{p_r}{p_l}\right)^{\frac{\gamma-1}{2\gamma}}-1\right] < 0$	(2.9a-gas)
		$p_l < p_r,\quad -\frac{2c_l}{\gamma-1}-\frac{2c_r}{\gamma-1} < u_l-u_r < \frac{2c_r}{\gamma-1}\left[\left(\frac{p_l}{p_r}\right)^{\frac{\gamma-1}{2\gamma}}-1\right] < 0$	(2.9b-gas)
2.4a-gas	$\overset{G}{R}\vert\overset{G}{R}$	$u_l-u_r < -\frac{2c_l}{\gamma-1}-\frac{2c_r}{\gamma-1}$	(2.10-gas)

across the interface is assured. This is not necessarily correct. As discussed above, the solution of a Riemann problem is related to not only the dynamic parameters such as pressure and velocity but also the thermal parameters such as temperature or entropy and the material properties in the EOS. In the singularity decomposition, the material properties play a very important role to determine the final interfacial dynamic parameters and entropy as discussed in Section 2. The conditions suggested and imposed on the ghost fluid status to be presented below in Section 3.1 for ensuring a successful GFM based algorithm are useful and can help to explain the efficiency and limitation for the GFM presented in [2,12,13,16] in particular, or may be employed to analyse other GFM based algorithm. The analysis is focused on the very earlier few steps of computation, especially the first two steps. It is these very earlier few steps that crucially determine whether the singularity is correctly decomposed.

3.1. An observation

From the observation shown in [20], an incorrect or inconsistent Riemann wave provided by one or both of the GFM Riemann problems in the respective real fluids may lead to inaccurate results provided by a GFM based method during the numerical decomposition of the singularity. Thus, under the imposition of continuity of pressure and velocity across the interface, we further propose/suggest that if the two GFM Riemann problems can provide consistent and correct Riemann waves in the respective real fluids during the numerical decomposition of the singularity, the GFM based algorithm should be able to generate acceptable results. Based on this suggestion and requiring that consistent Riemann waves be provided by the two GFM Riemann problems in the real fluids during the decomposition of the singularity, the following two conditions have to be satisfied and imposed on the ghost fluid status.

Table 3
Summary of equivalent Conclusions 2.1–2.4 for water–water Riemann problems and applicable for W*-W GFM Riemann problem in Section 3)

Conclusion	Solution type	Conditions	Equation
Category I			
2.1-water	${}^{W}_{R}\|^{W}_{S}$	$p_l > p_r,\quad \frac{2\bar{c}_l}{N-1}\left[\left(\frac{\bar{p}_r}{\bar{p}_l}\right)^{\frac{N-1}{2N}}-1\right] < u_l-u_r < \sqrt{\frac{\bar{p}_r}{\rho_r}}\sqrt{\frac{\bar{p}_l}{\bar{p}_r}-1}\sqrt{1-\left(\frac{\bar{p}_l}{\bar{p}_r}\right)^{-1/N}}$	(2.6-water)
2.1a-water	${}^{W}_{-}\|^{W}_{S}$	$p_l > p_r,\quad u_l-u_r = \sqrt{\frac{\bar{p}_r}{\rho_r}}\sqrt{\frac{\bar{p}_l}{\bar{p}_r}-1}\sqrt{1-\left(\frac{\bar{p}_l}{\bar{p}_r}\right)^{-1/N}} > 0$	(2.6a-water)
2.1b-water	${}^{W}_{R}\|^{W}_{-}$	$p_l > p_r,\quad u_l-u_r = \frac{2\bar{c}_l}{N-1}\left[\left(\frac{\bar{p}_r}{\bar{p}_l}\right)^{\frac{N-1}{2N}}-1\right] < 0$	(2.6b-water)
2.2-water	${}^{W}_{S}\|^{W}_{R}$	$p_l < p_r,\quad \frac{2\bar{c}_r}{N-1}\left[\left(\frac{\bar{p}_l}{\bar{p}_r}\right)^{\frac{N-1}{2N}}-1\right] < u_l-u_r < \sqrt{\frac{\bar{p}_l}{\rho_l}}\sqrt{\frac{\bar{p}_r}{\bar{p}_l}-1}\sqrt{1-\left(\frac{\bar{p}_r}{\bar{p}_l}\right)^{-1/N}}$	(2.7-water)
2.2a-water	${}^{W}_{S}\|^{W}_{-}$	$p_l < p_r,\quad u_l-u_r = \sqrt{\frac{\bar{p}_l}{\rho_l}}\sqrt{\frac{\bar{p}_r}{\bar{p}_l}-1}\sqrt{1-\left(\frac{\bar{p}_r}{\bar{p}_l}\right)^{-1/N}} > 0$	(2.7a-water)
2.2b-water	${}^{W}_{-}\|^{W}_{R}$	$p_l < p_r,\quad u_l-u_r = \frac{2\bar{c}_r}{N-1}\left[\left(\frac{\bar{p}_l}{\bar{p}_r}\right)^{\frac{N-1}{2N}}-1\right] < 0$	(2.7b-water)
Category II			
2.3-water	${}^{W}_{S}\|^{W}_{S}$	$p_l > p_r,\quad u_l-u_r > \sqrt{\frac{\bar{p}_r}{\rho_r}}\sqrt{\frac{\bar{p}_l}{\bar{p}_r}-1}\sqrt{1-\left(\frac{\bar{p}_l}{\bar{p}_r}\right)^{-1/N}} > 0$	(2.8a-water)
		$p_l < p_r,\quad u_l-u_r > \sqrt{\frac{\bar{p}_l}{\rho_l}}\sqrt{\frac{\bar{p}_r}{\bar{p}_l}-1}\sqrt{1-\left(\frac{\bar{p}_r}{\bar{p}_l}\right)^{-1/N}} > 0$	(2.8b-water)
Category III			
2.4-water	${}^{W}_{R}\|^{W}_{R}$	$p_l > p_r,\quad -\frac{2\bar{c}_l k_{cl}}{N-1}-\frac{2\bar{c}_r k_{cr}}{N-1} < u_l-u_r < \frac{2\bar{c}_l}{N-1}\left[\left(\frac{\bar{p}_r}{\bar{p}_l}\right)^{\frac{N-1}{2N}}-1\right] < 0$	(2.9a-water)
		$p_l < p_r,\quad -\frac{2\bar{c}_l k_{cl}}{N-1}-\frac{2\bar{c}_r k_{cr}}{N-1} < u_l-u_r < \frac{2\bar{c}_r}{N-1}\left[\left(\frac{\bar{p}_l}{\bar{p}_r}\right)^{\frac{N-1}{2N}}-1\right] < 0$	(2.9b-water)
2.4a-water	${}^{W}_{R}\|^{W}_{R}$	$u_l-u_r < -\frac{2\bar{c}_l k_{cl}}{N-1}-\frac{2\bar{c}_r k_{cr}}{N-1},\ k_{cl} = [1-(B/\bar{p}_l)^{\frac{N-1}{2N}}]$	(2.10-water)

Condition (I): the Riemann wave in the real fluid side for *both* GFM Riemann problems is initially consistent with that for the same side as for the original Riemann problem.
Condition (II): the new Riemann problem formed from the GFM computation maintains the same type of solution as that for the original Riemann problem during the decomposition of the singularity. In other words, Condition (I) is maintained after the first step of computation.

We shall impose these two Conditions on the ghost fluid status and then analyse and determine if these are satisfied for the various existing GFM based methods. One will then base on these two conditions to identify some of the range of conditions, where the existing GFM based algorithms are unable to provide correct and consistent Riemann waves in the real fluids and thus may lead to inaccurate results.

After the first step of computation, the results from the GFM computation form a new Riemann problem at the interface. The new Riemann problem may not maintain the same type of solution as that for the original Riemann problem due to the inaccurate boundary treatment at the interface. The imposition of Condition (II) ensures that a correct Riemann wave is always generated in the respective real fluids. As a result, the satisfying of Conditions (I) and (II) can ensure that the Riemann wave in the respective real fluids provided by the GFM Riemann problems is always consistent with that of the original Riemann problem during the numerical decomposition of the singularity.

The imposition of Condition (II) is strictly the adherence of Condition (I) at the first few steps of computation. It is not so straightforward to state the criterion for the enforcement of Condition (II) since the computation would involve the numerical scheme. Also, the status of the interface conditions according to (3.1a) for the gaseous side and (3.1b) for the water phase have some bearings on Condition (II). In this work, we suggest a possible means where analysis of the above-mentioned two interfacial states can serve

as a reasonable proxy on whether Condition (II) is likely to be satisfied. If the interfacial states according to (3.1a) and (3.1b) for the pressure and velocity are sufficiently close, it should lead to Condition (II) being fulfilled under the prior satisfaction of Condition (I). The increasing divergence of the interfacial states will lead to increasing magnitude of errors introduced or eventual breakdown. In practice, the numerical scheme selected with its accompanying (inherent) damping characteristics may mitigate the effect especially when the initial conditions imposed are deemed to be not so critical.

Obviously, the incorporation of Conditions (I) and (II) is dependent on the definition of the ghost fluid status. Except for the MGFM developed by Liu et al. [20] and the GFM algorithm by Aslam [3,4], where the Riemann solver is employed to define the ghost fluid status (globally for the latter while it is locally applied near the interface for the former), the general procedures used to define the ghost fluid status as found in the literature [2,5,12,13,16] are very similar to those presented in [5,12,13]. We, therefore, shall focus our analysis on the original GFM [12], the new version GFM [5,13] and the MGFM [20] in this work; the algorithm developed in [3,4] should be expected to give acceptable results under the tracking of both material interface and shock front for the Riemann problems discussed.

In the discussion below, we first verify the applicability of Condition (I) according to the specific definition of the ghost fluid status for each type of solution. If Condition (I) is violated, Condition (II) will not be further analysed as an incorrect Riemann wave is initially inherent and provided in one of the real fluids by the associated GFM algorithm. If Condition (I) is fulfilled for both GFM Riemann problems, we next check the satisfying of Condition (II) at the first step of calculation. This is done by ensuring that Condition (I) is also satisfied by both GFM Riemann problems after the first step of computation. If either Condition (I) or (II) are violated by either of the GFM Riemann problems, an incorrect or inconsistent Riemann wave is generated in the affected real fluid. As such, theoretically, errors will be incurred in computation although these errors may be well limited depending on the numerical scheme used. In the range of conditions, where either Condition (I) or (II) is violated, corresponding examples will be given in Section 4 for the associated GFM algorithm to illustrate the computed (inaccurate) results.

Before the detailed analysis, we first introduce two important inequalities which will be used in the coming discussion. By using functional and inequality analysis, the two inequalities, (3.2) and (3.3), are held. If $p > p_0$ and $\rho_{0w} > 0.5(\gamma+1)\rho_{0g}$, then

$$\sqrt{\frac{\bar{p}_0}{\rho_{0w}}}\sqrt{\frac{\bar{p}}{\bar{p}_0}-1}\sqrt{1-\left(\frac{\bar{p}}{\bar{p}_0}\right)^{-1/N}} < \sqrt{\frac{\beta p_0}{\rho_{0g}}}\frac{p/p_0-1}{\sqrt{1+\tau p/p_0}}. \tag{3.2}$$

On the other hand, if $p_0 > p$ and $\rho_{0w} > \frac{\gamma p_0}{N\bar{p}_0}\rho_{0g}$, then

$$\frac{2\bar{c}_{0w}}{N-1}\left[\left(\frac{\bar{p}}{\bar{p}_0}\right)^{\frac{N-1}{2N}}-1\right] > \frac{2c_{0g}}{\gamma-1}\left[\left(\frac{p}{p_0}\right)^{\frac{\gamma-1}{2\gamma}}-1\right]. \tag{3.3}$$

Here, ρ_{0g} and ρ_{0w} are the respective gas and water densities at pressure p_0; the subscripts "g" and "w" indicate "gas" and "water" media, respectively.

3.2. The original GFM on the gas–water Riemann problem: some analysis

In this subsection, we will discuss in detail the performance of the original GFM [12] for each solution type. For the original GFM, we have $p_r^* = p_r, u_r^* = u_r, p_l^* = p_l$ and $u_l^* = u_l$.

3.2.1. The solution type of (2.1) under consideration is $_R^G|_S^W$

We first check the satisfaction of Condition (I) and find the range of conditions, where Condition (I) is violated. For this type of solution, we have $p_l > p_r$ from Conclusion 2.1. Condition (I) requires that the

GFM Riemann problem (3.1a) "SHOULD" have a solution type of either ${}^{\mathrm{G}}_{\mathrm{R}}|^{\mathrm{G}*}_{\mathrm{S}}$ or ${}^{\mathrm{G}}_{\mathrm{R}}|^{\mathrm{G}*}_{\mathrm{R}}$, while the GFM Riemann problem (3.1b) "SHOULD" have a solution type of either ${}^{\mathrm{W}*}_{\mathrm{R}}|^{\mathrm{W}}_{\mathrm{S}}$ or ${}^{\mathrm{W}*}_{\mathrm{S}}|^{\mathrm{W}}_{\mathrm{S}}$. On the other hand, the solution types of ${}^{\mathrm{G}}_{\mathrm{R}}|^{\mathrm{G}*}_{\mathrm{R}}$ and ${}^{\mathrm{W}*}_{\mathrm{S}}|^{\mathrm{W}}_{\mathrm{S}}$ are excluded by inequality (2.6) of Conclusion 2.1. (That is, the respective necessary conditions, (2.9a-gas) and (2.8a-water), of generating ${}^{\mathrm{G}}_{\mathrm{R}}|^{\mathrm{G}*}_{\mathrm{R}}$ and ${}^{\mathrm{W}*}_{\mathrm{S}}|^{\mathrm{W}}_{\mathrm{S}}$ as shown in Tables 2 and 3 are applied and found to be inconsistent with inequality (2.6). Hereafter, similar equivalent Conclusions 2.1–2.4 for the single gas or water Riemann problem are applied in the discussion of the gaseous or water GFM Riemann problem.) Thus, the only acceptable solution type for (3.1a) is ${}^{\mathrm{G}}_{\mathrm{R}}|^{G*}_{S}$, which leads to

$$\frac{2c_{\mathrm{l}}}{\gamma-1}\left[\left(\frac{p_{\mathrm{r}}}{p_{\mathrm{l}}}\right)^{\frac{\gamma-1}{2\gamma}}-1\right] < u_{\mathrm{l}}-u_{\mathrm{r}} < \sqrt{\frac{\beta p_{\mathrm{r}}}{\rho^{*}_{\mathrm{r}}}}\frac{p_{\mathrm{l}}/p_{\mathrm{r}}-1}{\sqrt{1+\tau p_{\mathrm{l}}/p_{\mathrm{r}}}} \tag{3.4a}$$

because of inequality (2.6-gas) in Table 2. It is easy to verify that inequality (2.6) and inequality (3.2) ensure that inequality, (3.4a), is always true regardless. On the other hand, the admissible solution type for (3.1b) can be either ${}^{\mathrm{W}*}_{\mathrm{R}}|^{\mathrm{W}}_{\mathrm{S}}$ or ${}^{\mathrm{W}*}_{\mathrm{R}}|^{\mathrm{W}}_{\mathrm{R}}$ under the conditions given by inequality (2.6). In fact, if the flow initial conditions satisfy the following inequality (3.4b) (which is also inequality (2.6-water) listed in Table 3)

$$\frac{2\bar{c}^{*}_{\mathrm{l}}}{N-1}\left[\left(\frac{\bar{p}_{\mathrm{r}}}{\bar{p}_{\mathrm{l}}}\right)^{\frac{N-1}{2N}}-1\right] < u_{\mathrm{l}}-u_{\mathrm{r}} < \sqrt{\frac{\bar{p}_{\mathrm{r}}}{\rho_{\mathrm{r}}}}\sqrt{\frac{\bar{p}_{\mathrm{l}}}{\bar{p}_{\mathrm{r}}}-1}\sqrt{1-\left(\frac{\bar{p}_{\mathrm{l}}}{\bar{p}_{\mathrm{r}}}\right)^{-1/N}}, \tag{3.4b}$$

the solution type of (3.1b) is ${}^{\mathrm{W}*}_{\mathrm{R}}|^{\mathrm{W}}_{\mathrm{S}}$, while if they satisfy inequality (3.4c)

$$\frac{2c_{\mathrm{l}}}{\gamma-1}\left[\left(\frac{p_{\mathrm{r}}}{p_{\mathrm{l}}}\right)^{\frac{\gamma-1}{2\gamma}}-1\right] < u_{\mathrm{l}}-u_{\mathrm{r}} < \frac{2\bar{c}^{*}_{\mathrm{l}}}{N-1}\left[\left(\frac{\bar{p}_{\mathrm{r}}}{\bar{p}_{\mathrm{l}}}\right)^{\frac{N-1}{2N}}-1\right], \tag{3.4c}$$

the solution type of (3.1b) is ${}^{\mathrm{W}*}_{\mathrm{R}}|^{\mathrm{W}}_{\mathrm{R}}$. Under the conditions given by Conclusion 2.1, inequality (3.4c) results from inequality (2.9a-water) in Table 2 and inequality (3.3). Thus, Condition (I) is fulfilled if the flow initial conditions satisfy inequality (3.4b), while it is violated if they satisfy inequality (3.4c). This violation of Condition (I) leads to the generation of a rarefaction wave in the water flow. Physically, a compressive wave (shock) should propagate for this type solution considered.

One should note that if (3.4b) is held the two GFM Riemann problems are able to satisfy Condition (I) initially. However, Condition (II) may not be maintained because the interface velocities and pressures provided by the respective GFM Riemann problems may be very different due to the large difference of inertia between the gas and the water medium. The interfacial pressures and velocities obtained by (3.1a) and (3.1b) can be far from each other (see [20] for a shock impacting on the gas–water interface). This incompatibility of (3.1a) and (3.1b) at the interface can result in a large positive value of $u_{\mathrm{l}}-u_{\mathrm{r}}$ at the next step computation, attributable to the relatively larger increase of the interface velocity through (3.1a) in comparison to that produced by (3.1b); here, Conclusion 2.6 is used. Furthermore, due to the very large B appearing in the Tait EOS, the right-hand side of (3.4b) is relatively very close to zero and the said inequality can then be violated easily, unless a large pressure is initially given to the gas medium. Thus, an inconsistent Riemann wave incurs in the water flow. That is, initially a compressive wave is generated in water by (3.1b) following the flow initial condition satisfying inequality (3.4b), while a rarefaction wave is provided by (3.1b) later after the first step of computation. Such inconsistency usually leads to numerical oscillations. After the satisfaction of Condition (I) as applicable for both media, one still needs to maintain Condition (II) via the two GFM Riemann problems to provide the interfacial states close to each other. In other words, (3.1a) of the solution type ${}^{\mathrm{G}}_{\mathrm{R}}|^{G*}_{S}$ is required to provide interfacial pressure and velocity close to those provided by (3.1b) of the solution type ${}^{\mathrm{W}*}_{\mathrm{R}}|^{\mathrm{W}}_{\mathrm{S}}$; this leads to

$$\sqrt{\frac{\bar{p}_{\mathrm{r}}}{\rho_{\mathrm{r}}}}\sqrt{\frac{\bar{p}}{\bar{p}_{\mathrm{r}}}-1}\sqrt{1-\left(\frac{\bar{p}}{\bar{p}_{\mathrm{r}}}\right)^{-1/N}} \approx \sqrt{\frac{\beta p_{\mathrm{r}}}{\rho^{*}_{\mathrm{r}}}}\frac{p/p_{\mathrm{r}}-1}{\sqrt{1+\tau p/p_{\mathrm{r}}}} \quad \text{for } p_{\mathrm{r}} \leqslant p. \tag{3.5}$$

Obviously (3.5) is true when $p_r \approx p$; (3.5) takes on equality only when $p_r = p$ due to inequality (3.2). By a simple functional analysis, (3.5) can also be true if $\rho_r \approx 0.5(\gamma+1)\rho_r^*$ for p far larger than p_r. It means that the initial gas density (ghost fluid) should be comparable to or larger than the water density or p and p_r are very close to each other for ensuring Condition (II) is fulfilled. The former implies that an initially very high pressure and density is required for the gas, while the latter indicates that the interface is in normal motion. Either one of these two situations together with the satisfying of Condition (I) can ensure correct and consistent Riemann waves as provided by the original GFM in the respective real fluids. Numerical tests showed that perceptibly large errors are likely to occur if the ratio of water density to the initial gas density is higher than about 100 using the original GFM. It may be mentioned that if Condition (I) is violated, inaccurate results may prevail even if the initial $\rho_l \approx \rho_r$ is true (see Case 2 in Section 4).

3.2.2. The solution type of (2.1) is ${}^{G}_{S}|^{W}_{R}$

For this type of solution, we have $p_l < p_r$ from Conclusion 2.2. By similar analysis as carried out in Section 3.2.1, the only acceptable solution for (3.1a) is ${}^{G}_{S}|^{G*}_{R}$ under Condition (I). This results in

$$\frac{2c_r^*}{\gamma-1}\left[\left(\frac{p_l}{p_r}\right)^{\frac{\gamma-1}{2\gamma}}-1\right] < u_l - u_r < \sqrt{\frac{\beta p_l}{\rho_l}}\frac{p_r/p_l-1}{\sqrt{1+\tau p_r/p_l}} \tag{3.6a}$$

due to (2.7-gas) in Table 2. On the other hand, under the inequality (2.7), the solution type of (3.1b) can only be either ${}^{W*}_{S}|^{W}_{R}$ or ${}^{W*}_{S}|^{W}_{S}$; if the following

$$\frac{2\bar{c}_r}{N-1}\left[\left(\frac{\bar{p}_l}{\bar{p}_r}\right)^{\frac{N-1}{2N}}-1\right] < u_l - u_r < \sqrt{\frac{\bar{p}_l}{\rho_l^*}}\sqrt{\frac{\bar{p}_r}{\bar{p}_l}-1}\sqrt{1-\left(\frac{\bar{p}_r}{\bar{p}_l}\right)^{-1/N}} \tag{3.6b}$$

is satisfied (which is (2.7-water) in Table 3), the solution type of (3.1b) is ${}^{W*}_{S}|^{W}_{R}$, while it is ${}^{W*}_{S}|^{W}_{S}$ if the following inequality (3.6c) is held

$$\sqrt{\frac{\bar{p}_l}{\rho_l^*}}\sqrt{\frac{\bar{p}_r}{\bar{p}_l}-1}\sqrt{1-\left(\frac{\bar{p}_r}{\bar{p}_l}\right)^{-1/N}} < u_l - u_r < \sqrt{\frac{\beta p_l}{\rho_l}}\frac{p_r/p_l-1}{\sqrt{1+\tau p_r/p_l}}. \tag{3.6c}$$

Under Conclusion 2.2, inequality (3.6c) results from (2.8b-water) in Table 3 and inequality (3.2). Inequality (3.2) together with inequality (2.7) always gives rise to the satisfying of (3.6a). Thus, Condition (I) is fulfilled if the flow initial conditions satisfy inequality (3.6b), while it is violated if they satisfy inequality (3.6c). Similar to the above analysis in Section 3.2.1, inequality (3.6b) is very easily violated in the next step computation, unless the initial gas has a very high pressure and a density comparable to or larger than the water density or the interface is in normal motion.

3.2.3. The solution type of (2.1) under consideration is ${}^{G}_{S}|^{W}_{S}$

For $p_l > p_r$, because of the conditions given by inequality (2.8a) of Conclusion 2.3, to meet Condition (I), only ${}^{G}_{S}|^{G*}_{S}$ and ${}^{W*}_{S}|^{W}_{S}$ are acceptable for the respective two GFM Riemann problems. Inequalities (2.8a-gas) in Table 2 and (2.8a-water) in Table 3 lead to

$$u_l - u_r > \sqrt{\frac{\beta p_r}{\rho_r^*}}\frac{p_l/p_r-1}{\sqrt{1+\tau p_l/p_r}}, \tag{3.7a}$$

$$u_l - u_r > \sqrt{\frac{\bar{p}_r}{\rho_r}}\sqrt{\frac{\bar{p}_l}{\bar{p}_r}-1}\sqrt{1-\left(\frac{\bar{p}_l}{\bar{p}_r}\right)^{-1/N}}, \tag{3.7b}$$

respectively. Inequality (3.7b) is always true due to inequality (3.2) and the conditions given by inequality (2.8a), while (3.7a) may not be so. In fact, under the following condition (3.7c) for $p_l > p_r$, the solution type of (3.1a) is ${}^{G}_{R}|^{G*}_{S}$. The inequality,

$$\sqrt{\frac{\bar{p}_r}{\rho_r}}\sqrt{\frac{\bar{p}_l}{\bar{p}_r}-1}\sqrt{1-\left(\frac{\bar{p}_l}{\bar{p}_r}\right)^{-1/N}} < u_l - u_r < \sqrt{\frac{\beta p_r}{\rho_r^*}}\frac{p_l/p_r - 1}{\sqrt{1+\tau p_l/p_r}}, \tag{3.7c}$$

comes from inequality (2.6-gas) in Table 2 and inequality (3.2). The satisfying of (3.7c) for flow initial conditions leads to the violation of Condition (I).

For $p_l < p_r$, it can be shown that the admissible solution types for the respective two GFM Riemann problems are ${}^{G}_{S}|^{G*}_{S}$ and ${}^{W*}_{S}|^{W}_{S}$ under the conditions given by inequality (2.8b), resulting in

$$u_l - u_r > \sqrt{\frac{\beta p_l}{\rho_l}}\frac{p_r/p_l - 1}{\sqrt{1+\tau p_r/p_l}}, \tag{3.7d}$$

$$u_l - u_r > \sqrt{\frac{\bar{p}_l}{\rho_l^*}}\sqrt{\frac{\bar{p}_r}{\bar{p}_l}-1}\sqrt{1-\left(\frac{\bar{p}_r}{\bar{p}_l}\right)^{-1/N}}, \tag{3.7e}$$

from the respective (2.8b-gas) in Table 2 and (2.8b-water) in Table 3. Conditions (3.7d) and (3.7e) are always held due to inequality (3.2) and the conditions given by inequality (2.8b). As a result, Condition (I) is satisfied initially for $p_l < p_r$. Similar to above analysis, Condition (II) can be easily violated due to the violation of inequality (3.7b) or (3.7e) after the first step computation. The maintenance of Condition (II) usually requires very high pressure and density in gas, or the interface in normal motion.

3.2.4. The solution type of (2.1) under investigation is ${}^{G}_{R}|^{W}_{R}$

For $p_l > p_r$, it can be shown that the admissible solution types for the respective two GFM Riemann problems are ${}^{G}_{R}|^{G*}_{R}$ and ${}^{W}_{R}|^{W*}_{R}$ under the conditions given by inequality (2.9a) of Conclusion 2.4. This leads to

$$-\frac{2c_l}{\gamma-1} - \frac{2c_r^*}{\gamma-1} < u_l - u_r < \frac{2c_l}{\gamma-1}\left[\left(\frac{p_r}{p_l}\right)^{\frac{\gamma-1}{2\gamma}} - 1\right], \tag{3.8a}$$

$$-\frac{2\bar{c}_l^* k_{cl}}{N-1} - \frac{2\bar{c}_r k_{cr}}{N-1} < u_l - u_r < \frac{2\bar{c}_l^*}{N-1}\left[\left(\frac{\bar{p}_r}{\bar{p}_l}\right)^{\frac{N-1}{2N}} - 1\right], \tag{3.8b}$$

from (2.9a-gas) in Table 2 and (2.9a-water) in Table 3, respectively. Here, $k_{cl} = [1 - (B/\bar{p}_l)^{\frac{N-1}{2N}}]$. It is easy to check that (3.8a) and (3.8b) are always held due to inequality (3.3) and the conditions given by inequality (2.9a). As a result, Condition (I) is satisfied initially for $p_l > p_r$.

For $p_l < p_r$, only ${}^{G}_{R}|^{G*}_{R}$ and ${}^{W*}_{R}|^{W}_{R}$ are acceptable for the respective two GFM Riemann problems to meet Condition (I). This leads to

$$-\frac{2c_l}{\gamma-1} - \frac{2c_r^*}{\gamma-1} < u_l - u_r < \frac{2c_r^*}{\gamma-1}\left[\left(\frac{p_l}{p_r}\right)^{\frac{\gamma-1}{2\gamma}} - 1\right], \tag{3.8c}$$

$$-\frac{2\bar{c}_l^* k_{cl}}{N-1} - \frac{2\bar{c}_r k_{cr}}{N-1} < u_l - u_r < \frac{2\bar{c}_r}{N-1}\left[\left(\frac{\bar{p}_l}{\bar{p}_r}\right)^{\frac{N-1}{2N}} - 1\right] \tag{3.8d}$$

from (2.9b-gas) in Table 2 and (2.9b-water) in Table 3. On the other hand, if the following condition (3.8e) is held for $p_l < p_r$,

$$\frac{2c_r^*}{\gamma-1}\left[\left(\frac{p_l}{p_r}\right)^{\frac{\gamma-1}{2\gamma}}-1\right] < u_l - u_r < \frac{2\bar{c}_r}{N-1}\left[\left(\frac{\bar{p}_l}{\bar{p}_r}\right)^{\frac{N-1}{2N}}-1\right], \tag{3.8e}$$

the solution type of (3.1a) is ${}^{G}_{S}|^{G*}_{R}$. Under the conditions given by Conclusion 2.4, (3.8e) is admissible and obtained from inequality (2.7-gas) and inequality (3.3). Thus, the satisfying of (3.8e) for flow initial conditions leads to the violation of Condition (I). Similarly, (3.8b) or (3.8d) is very easily violated after the first step computation and can lead to the violation of Condition (II) unless the two GFM Riemann problems can provide close interface states. This latter can be materialised provided

$$\frac{2c_r^*}{\gamma-1}\left[\left(\frac{p}{p_r}\right)^{\frac{\gamma-1}{2\gamma}}-1\right] \approx \frac{2\bar{c}_r}{N-1}\left[\left(\frac{\bar{p}}{\bar{p}_r}\right)^{\frac{N-1}{2N}}-1\right] \quad \text{for } p \leqslant p_r, \tag{3.9}$$

which further leads to $\rho_r \approx \frac{\gamma p_r}{N\bar{p}_r}\rho_r^*$ if p is far smaller than p_r, or $p \approx p_r$. In other words, the initial density for the gas should be far larger than the water density if p is not close to p_r. It implies that in any realistic situation, where p is not close to p_r, the original GFM is not likely able to maintain Condition (II) and then provide an incorrect or inconsistent Riemann wave in one of the real fluids, which may lead to error-borne results for this type of solution.

Detailed analysis and discussion have been carried out above for the original GFM. Here, we would like to give a very brief summary.

Conclusion 3.1. *On the use of the original GFM*,

(1) *There is a range of conditions for each type solution such that the original GFM is inherently unable to provide the correct Riemann wave in one real fluid during the numerical decomposition of the singularity. The range is defined by* (3.4c), (3.6c), (3.7c) *or* (3.8e), *respectively.*
(2) *For Category I and Category II solutions, the original GFM is able to provide correct and consistent Riemann waves in the respective real fluids for those problems with initial very high gas pressure and a density sufficiently comparable to or larger than the water density under the consideration of satisfying Condition* (*I*).
(3) *For Category III, the original GFM can provide a consistent Riemann wave in the respective real fluids if the initial gas density is far higher than the water density under the consideration of satisfying Condition* (*II*), *provided Condition* (*I*) *is first satisfied.*

3.3. The new version GFM on the gas–water Riemann problem: some analysis

For the new version GFM [5,13], we have $p_r^* = p_l$, $u_r^* = u_r$, $p_l^* = p_l$ and $u_l^* = u_r$, and the two associated GFM Riemann problems are very different from the counterpart of the original GFM; Riemann problem (3.1a) is of constant pressure while Riemann problem (3.1b) is of constant velocity. We, thus, have the following from Conclusion 2.5.

Conclusion 3.2. *Using the new version GFM, the GFM Riemann problem* (3.1a) *provides a solution type of either Category II or Category III depending on* $u_l - u_r > 0$ *or* $u_l - u_r < 0$, *respectively. The GFM Riemann problem*(3.1b) *always provides a solution type of Category I with a rarefaction wave in the high-pressure side and a shock wave in the low-pressure side.*

From Conclusion 3.2, the GFM Riemann problem (3.1b) can provide only Category I solution, while the GFM Riemann problem (3.1a) is unable to provide Category I solution. This is unlike the original GFM, where all type solutions are admissible for both (3.1a) and (3.1b). Furthermore, it can be shown that (3.1a) always provides an interfacial velocity of

$$u_{\mathrm{I}}^{\mathrm{G}} = 0.5(u_{\mathrm{l}} + u_{\mathrm{r}}), \tag{3.10}$$

irrespective of the solution type being ${}^{\mathrm{G}}_{\mathrm{R}}|^{\mathrm{G*}}_{\mathrm{R}}$ (Category III) or ${}^{\mathrm{G}}_{\mathrm{S}}|^{\mathrm{G*}}_{\mathrm{S}}$ (Category II) using the new version GFM. In a similar way as carried out in Section 3.2, we now analyse the performance of the new version GFM for each type of solution.

3.3.1. The solution type of (2.1) under consideration is ${}^{G}_{R}|^{W}_{S}$

For this type of solution, we have $p_{\mathrm{l}} > p_{\mathrm{r}}$ from Conclusion 2.1. From Conclusion 3.2, ${}^{\mathrm{W*}}_{\mathrm{R}}|^{\mathrm{W}}_{\mathrm{S}}$ is the only solution type provided by (3.1b), which results in a correct Riemann wave provided in the real fluid (water); if $u_{\mathrm{l}} - u_{\mathrm{r}} < 0$, (3.1a) provides a solution type of ${}^{\mathrm{G}}_{\mathrm{R}}|^{\mathrm{G*}}_{\mathrm{R}}$, while it provides a solution type of ${}^{\mathrm{G}}_{\mathrm{S}}|^{\mathrm{G*}}_{\mathrm{S}}$ if $u_{\mathrm{l}} - u_{\mathrm{r}} > 0$. Thus, under the condition of $u_{\mathrm{l}} - u_{\mathrm{r}} < 0$, Condition (I) is maintained, while it is violated if $u_{\mathrm{l}} - u_{\mathrm{r}} > 0$. Next we check the maintenance of Condition (II) for the solution type of ${}^{\mathrm{G}}_{\mathrm{R}}|^{\mathrm{G*}}_{\mathrm{R}}$ which has already satisfied Condition (I) for both GFM Riemann problems. It can be easily shown that the interfacial pressure provided by (3.1a) is

$$p_{\mathrm{I}}^{\mathrm{G}} = p_{\mathrm{L}}\left[1 + \frac{\gamma - 1}{4c_{\mathrm{l}}}(u_{\mathrm{l}} - u_{\mathrm{r}})\right]^{2\gamma/(\gamma-1)}. \tag{3.11}$$

In order that Condition (II) is satisfied, a requirement is that the two GFM Riemann problems provide interfacial states close to each other. By assuming (3.1b) provides an interfacial velocity close to (3.10), it can be suggested that the interfacial pressure obtained by (3.1b) is close to

$$\bar{p}_{\mathrm{I}}^{\mathrm{W}} = \bar{p}_{\mathrm{L}}\left[1 - \frac{N - 1}{4\bar{c}_{\mathrm{l}}^{*}}(u_{\mathrm{l}} - u_{\mathrm{r}})\right]^{2N/(N-1)}. \tag{3.12}$$

(3.11) and (3.12) give the interfacial pressure value close to each other if $u_{\mathrm{l}} \approx u_{\mathrm{r}}$; an apparent initial large difference between u_{l} and u_{r} may lead to the violation of Condition (II). Numerical tests will show that inaccurate results are obtained when the difference between u_{l} and u_{r} is large.

3.3.2. The solution of (2.1) under consideration is ${}^{G}_{S}|^{W}_{R}$

For this type of solution, we have $p_{\mathrm{l}} < p_{\mathrm{r}}$ from inequality (2.7). From Conclusion 3.2, ${}^{\mathrm{W*}}_{\mathrm{S}}|^{\mathrm{W}}_{\mathrm{R}}$ is the only solution type provided by (3.1b), which results in a correct Riemann wave provided in the real fluid (water); if $u_{\mathrm{l}} - u_{\mathrm{r}} < 0$, (3.1a) provides a solution type of ${}^{\mathrm{G}}_{\mathrm{R}}|^{\mathrm{G*}}_{\mathrm{R}}$, while if $u_{\mathrm{l}} - u_{\mathrm{r}} > 0$ it provides a solution type of ${}^{\mathrm{G}}_{\mathrm{S}}|^{\mathrm{G*}}_{\mathrm{S}}$. Thus, under the condition of $u_{\mathrm{l}} - u_{\mathrm{r}} > 0$, Condition (I) is maintained, while it is violated if $u_{\mathrm{l}} - u_{\mathrm{r}} < 0$. It can be further checked that the necessity for the satisfying of Condition (II) is $u_{\mathrm{l}} - u_{\mathrm{r}} > 0$ using (3.10) and Conclusion 2.6.

3.3.3. The solution of (2.1) under consideration is ${}^{G}_{S}|^{W}_{R}$

For this type of solution, $u_{\mathrm{l}} - u_{\mathrm{r}} > 0$ must be held from Conclusion 2.3. As a result, the GFM Riemann (3.1a) always provides a solution type of ${}^{\mathrm{G}}_{\mathrm{S}}|^{\mathrm{G*}}_{\mathrm{S}}$, resulting in a correct Riemann wave provided in the gas from Conclusion 3.2. Furthermore, the GFM Riemann problem (3.1b) provides a solution type of ${}^{\mathrm{W*}}_{\mathrm{R}}|^{\mathrm{W}}_{\mathrm{S}}$ under $p_{\mathrm{l}} > p_{\mathrm{r}}$, while it provides a solution type of ${}^{\mathrm{W*}}_{\mathrm{S}}|^{\mathrm{W}}_{\mathrm{R}}$ under $p_{\mathrm{l}} < p_{\mathrm{r}}$. Thus, we can deduce that Condition (I) is satisfied if $p_{\mathrm{l}} > p_{\mathrm{r}}$, while it is violated if $p_{\mathrm{l}} < p_{\mathrm{r}}$. It is very interesting to note that, under the satisfying of Condition (I) ($p_{\mathrm{l}} > p_{\mathrm{r}}$), Condition (II) is generally violated for this type of solution. In fact, (3.1a) provides an interfacial velocity $u_{\mathrm{I}}^{\mathrm{G}} = 0.5(u_{\mathrm{l}} + u_{\mathrm{r}})$ and pressure $p_{\mathrm{I}}^{\mathrm{G}} > p_{\mathrm{l}}$, while (3.1b) generates an interfacial velocity

$u_{\mathrm{I}}^{\mathrm{W}} > u_{\mathrm{l}}$ and pressure $p_{\mathrm{I}}^{\mathrm{W}} < p_{\mathrm{l}}$ from Conclusion 2.6 and expression (3.10). This leads to an incorrect Riemann wave (rarefaction) provided in the gas in the next step computation.

3.3.4. The solution of (2.1) under consideration is $\overset{G}{R}|\overset{W}{R}$

For this type of solution, condition $u_{\mathrm{l}} - u_{\mathrm{r}} < 0$ must be satisfied from Conclusion 2.4. Because of Conclusion 3.2, the GFM Riemann problem (3.1a) can provide a correct Riemann wave in the gas; the GFM Riemann problem (3.1b) provides a solution type of $\overset{\mathrm{W}*}{\mathrm{R}}|\overset{\mathrm{W}}{\mathrm{S}}$ under $p_{\mathrm{l}} > p_{\mathrm{r}}$, while it provides a solution type of $\overset{\mathrm{W}*}{\mathrm{S}}|\overset{\mathrm{W}}{\mathrm{R}}$ under $p_{\mathrm{l}} < p_{\mathrm{r}}$. Thus, Condition (I) is satisfied if $p_{\mathrm{l}} < p_{\mathrm{r}}$, while it is violated if $p_{\mathrm{l}} > p_r$. Similar to the argument for Category II solution in Section 3.3.3, under the satisfying of Condition (I) ($p_l < p_{\mathrm{r}}$), Condition (II) is generally violated for Category III solution.

Here, we summarise some other important conclusions obtained:

Conclusion 3.3. *On the use of the new version GFM,*

(1) *There is a range for each type solution such that the new version GFM is inherently unable to provide the correct Riemann waves in one real fluid. The range is defined by* $u_{\mathrm{l}} - u_{\mathrm{r}} > 0$ *for* $\overset{\mathrm{G}}{\mathrm{R}}|\overset{\mathrm{W}}{\mathrm{S}}$, $u_{\mathrm{l}} - u_{\mathrm{r}} < 0$ *for* $\overset{\mathrm{G}}{\mathrm{S}}|\overset{\mathrm{W}}{\mathrm{R}}$, $u_{\mathrm{l}} - u_{\mathrm{r}} < 0$ *and* $p_{\mathrm{l}} > p_{\mathrm{r}}$ *for* $\overset{\mathrm{G}}{\mathrm{S}}|\overset{\mathrm{W}}{\mathrm{S}}$, *and* $u_{\mathrm{l}} - u_{\mathrm{r}} < 0$ *and* $p_{\mathrm{l}} > p_{\mathrm{r}}$ *for* $\overset{\mathrm{G}}{\mathrm{R}}|\overset{\mathrm{W}}{\mathrm{R}}$, *respectively*

(2) *For* $\overset{\mathrm{G}}{\mathrm{R}}|\overset{\mathrm{W}}{\mathrm{S}}$, *the new version GFM is able to provide correct and consistent Riemann waves in the respective real fluids given* u_l *and* u_{r} *are close to each other initially under the maintenance of Condition*(*I*); *for* $\overset{\mathrm{G}}{\mathrm{S}}|\overset{\mathrm{W}}{\mathrm{R}}$, *the necessary condition that the new version GFM is able to provide correct and consistent Riemann waves in the respective real fluids is* $u_{\mathrm{l}} - u_{\mathrm{r}} > 0$.

(3) *For Category II and Category III solutions, upon the satisfying of Condition* (*I*), *Condition* (*II*) *is generally not maintained.*

3.4. The MGFM on the gas–water Riemann problem: some analysis

The MGFM presented by Liu et al [20] has been shown to be able to handle those problems of shock impacting on an interface successfully. The basic idea of the MGFM is to predict the interface status using two nonlinear characteristics intersecting at the interface by an approximate Riemann problem solver (ARPS) developed in [18]. It has been shown that the interfacial status predicted using ARPS is second-order accurate and exact, respectively, for Category I and Category II solutions and the ARPS works even more efficiently when applied to gas–water flow [18]. Because the ghost fluid status in the MGFM cannot be expressed explicitly, it is not trivial to have a theoretical analysis to determine if the MGFM can provide correct and consistent Riemann waves in the respective real fluids. Extensive numerical tests, however, have shown that the MGFM is very likely able to provide acceptable results for Category I and Category II solutions. As for Category III solution, it can be noted that negative interfacial pressure can be provided by the ARPS if

$$u_{\mathrm{l}} - u_{\mathrm{r}} < -\sqrt{\frac{2p_{\mathrm{l}}/\rho_{\mathrm{l}}}{\gamma - 1}} - \sqrt{\frac{p_{\mathrm{r}}[(B/\bar{p}_{\mathrm{r}})^{-1/N} - 1]}{\rho_{\mathrm{r}}}}. \tag{3.13}$$

Thus, the MGFM is unable to provide correct solution if initial flow conditions follow

$$-\frac{2c_{\mathrm{l}}}{\gamma - 1} - \frac{2\bar{c}_{\mathrm{r}}k_{\mathrm{cr}}}{N - 1} < u_{\mathrm{l}} - u_{\mathrm{r}} < -\sqrt{\frac{2p_{\mathrm{l}}/\rho_{\mathrm{l}}}{(\gamma - 1)}} - \sqrt{\frac{p_{\mathrm{r}}[(B/\bar{p}_{\mathrm{r}})^{-1/N} - 1]}{\rho_{\mathrm{r}}}}. \tag{3.14}$$

The satisfying of (3.14) implies that the flow approaches cavitation condition. To avoid this difficulty, one can solve for a double rarefaction Riemann problem instead of the ARPS to obtain the exact interfacial

status in such situations. As pointed out in [8], once the flow approaches cavitation condition, the numerical schemes may encounter other difficulties. On the other hand, an exact interfacial status obtained to provide the ghost fluid status continues to ensure that the GFM based algorithm is able to proceed in such extreme conditions and with reasonable results.

3.5. The GFM algorithm on the special types of solution

In Section 2, four special types of solution, namely, $\overset{\mathrm{G}}{-}\big|^{\mathrm{W}}_{\mathrm{S}}$, $\overset{\mathrm{G}}{\mathrm{R}}\big|^{\mathrm{W}}_{-}$, $\overset{\mathrm{G}}{-}\big|^{\mathrm{W}}_{\mathrm{R}}$ and $\overset{\mathrm{G}}{\mathrm{S}}\big|^{\mathrm{W}}_{-}$ are introduced with the conditions provided for generating them. These four types of solution are similar to the shock impedance matching problems as discussed in [20]. Such conditions are very difficult to maintain and enforce by the GFM algorithm due to its manner of obtaining solution via computation in the single-medium flow. Condition (I) is generally violated by the GFM based algorithm [20]. As a result, unphysical wave reflection is usually generated on the side, where there is supposed to be no Riemann wave. This difficulty is unique for the GFM based algorithm. Even the MGFM developed in [20] is not completely able to remove the nonphysical reflection. Here, we would like to discuss in some details about the behaviour of the original and new version GFMs applied to these four special types of solution.

For $\overset{\mathrm{G}}{-}\big|^{\mathrm{W}}_{\mathrm{S}}$, Conclusion 2.2 shows that $p_{\mathrm{l}} > p_{\mathrm{r}}$ and $u_{\mathrm{l}} - u_{\mathrm{r}} > 0$. It is easy to show that a rarefaction wave is generated by (3.1a) in the real fluid (gas) using the original GFM. As a result, an unphysical hump (overshoot) in the velocity and a trough (undershoot) in the pressure are provided. On the other hand, a compressive wave is generated by (3.1a) in the real fluid (gas) using the new version GFM, resulting in an unphysical velocity trough (undershoot) and a pressure hump (overshoot).

For $\overset{\mathrm{G}}{\mathrm{R}}\big|^{\mathrm{W}}_{-}$, Conclusion (2.1b) shows that $p_{\mathrm{l}} < p_{\mathrm{r}}$ and $u_{\mathrm{l}} - u_{\mathrm{r}} < 0$. A rarefaction wave is generated by (3.1b) in the real fluid (water) using the original GFM. As a result, an unphysical hump (overshoot) in the velocity and a trough (undershoot) in the pressure ensue. On the other hand, a compressive wave is generated by (3.1b) in the real fluid (water) using the new version GFM, resulting in an unphysical velocity trough (undershoot) and a pressure hump (overshoot).

For $\overset{\mathrm{G}}{-}\big|^{\mathrm{W}}_{\mathrm{R}}$ and $\overset{\mathrm{G}}{\mathrm{S}}\big|^{\mathrm{W}}_{-}$, Conclusions 2.2b and 2.2 hold that $p_{\mathrm{l}} < p_{\mathrm{r}}$. A compressive wave is generated in the side, where it is supposed to be no Riemann wave using the original GFM. As a result, an unphysical trough (undershoot) in the velocity and a hump (overshoot) in the pressure are provided. On the other hand, a rarefaction wave is generated in this said side using the new version GFM, resulting in an unphysical velocity hump (overshoot) and a pressure trough (undershoot).

It should be noted that the isobaric fix is not directly referred to in the discussion on whether Condition (I) or (II) is affected. Without considering the influence of isobaric fix, it is still mathematically difficult to show conclusively if the maintenance of Conditions (I) and (II) is sufficient to ensure correct results provided by the GFM based method although the Conditions can ensure the correct Riemann waves are provided for by the GFM Riemann problems. Our extensive numerical tests have shown that the GFM based methods as discussed above are very likely able to provide acceptable results under maintenance of Conditions (I) and (II) using isentropic fix.

4. Numerical examples

Various gas–water Riemann problems can be constructed to support the analysis and conclusions reached in Section 3. These problems are constructed in the ranges where either the original GFM or the new version GFM or both are unable to maintain Condition (I) or (II). It has been found that, under such range of conditions, there are examples that inaccurate results are provided by the associated GFM algorithms. In parallel, the MGFM is employed for comparison. In the MGFM, the exact Riemann solution of double rarefaction wave is employed to provide the ghost fluid status once the ARPS predicts an

interfacial pressure lower than $0.5\min(p_l,p_r)$ initially. All computations are done using the second-order MUSCL with CFL = 0.9 and 201 uniform mesh points in domain [0,1]; the gas–water interface is located at 0.4 initially unless otherwise noted. The interface is captured using the level-set technique developed in [18] with re-initialisation. γ is always set to 1.4. All the parameters are made non-dimensional. All numerical results presented are at the moment of 100-time steps. For comparison, usually either the pressure or velocity profile (where inaccuracy is observed) is presented. No comparison or discussion is provided for those problems where *either* the original or new version GFMs can give acceptable results.

It is perhaps important to note that the successfully computed gas–water problems in Examples 4, 5, 6 as discussed in [12] satisfy Conditions (I) and (II) for both the original and new version GFM. Example 4 in [12] is a Riemann problem of solution type $\mathrm{G}_{\mathrm{R}}|^{\mathrm{W}}_{\mathrm{S}}$ with a very high pressure in gas, the initial gas density larger than water density and initial zero-velocity difference; Examples 5 and 6 are cases where the initial gas–water interfaces are in normal motion. Problems 2 and 3 as discussed in [20] satisfy Conditions (I) and (II) for both the original and new version GFM; Problems 7 and 8 in [20] violate Condition (I) for the original GFM; for the new version GFM, Problem 7 satisfies Condition (I) but violates Condition (II), and Problem 8 maintains both.

The MGFM can provide relatively excellent numerical results for all the examples to be presented below. The examples are presented in the order of the solution type. Although the theoretical analysis carried out and conclusions made in the present work are independent of the numerical scheme used, it may be noted that the extent and magnitude of numerical accuracy encountered are most likely dependent on the actual numerical solver employed. For ease of reference, we summarize all the examples in Table 4.

Case 1. This is a problem of solution type $\mathrm{G}_{\mathrm{R}}|^{\mathrm{W}}_{\mathrm{S}}$. The initial conditions are $u_l = 10.0$, $p_l = 1800.0$, $\rho_l = 0.2$ and $u_r = 0.0$, $p_r = 1.0$, $\rho_r = 1.0$. Condition (II) is violated by the original GFM attributable to the initial gas density quite smaller than the water density. The velocity profile provided by the original GFM is incorrect in the rarefaction wave region (see Fig. 1(a)); inaccurate shock wave position is also provided by the MUSCL-based original GFM. As for the new version GFM, Condition (I) is violated due to $u_l - u_r > 0$. Unacceptable result in the rarefaction wave region is also provided by the new version GFM as shown in Fig. 1(b). A reasonable velocity profile is provided by the MGFM and shown in Fig. 1(c).

Case 2. This is also a problem of solution type $\mathrm{G}_{\mathrm{R}}|^{\mathrm{W}}_{\mathrm{S}}$. The initial conditions are $u_l = -100.0$, $p_l = 8000.0$, $\rho_l = 1.2$ and $u_r = 0.0$, $p_r = 1.0$, $\rho_r = 1.0$. The initial gas–water interface is located at 0.5. Condition (I) is violated by the original GFM. Although the initial gas density is set to be larger than the water density, the original GFM is still unable to provide meaningful results. In fact, because the GFM Riemann problem (3.1b) provides a solution with spurious cavitation, the MUSCL-based original GFM computation col-

Table 4
Summary of examples

Problems	Original GFM			New version GFM		
	Condition (I)	Condition (II)	Accuracy	Condition (I)	Condition (II)	Accuracy
Case 1	√	×	×	×		×
Case 2	×		×	√	×	×
Case 3	×		×	√	×	×
Case 4	√	×	×	×		×
Case 5	√	×	×	×		×
Cases 6–9	×		×	×		×

√– Condition (I) or (II) satisfied or accurate results provided.

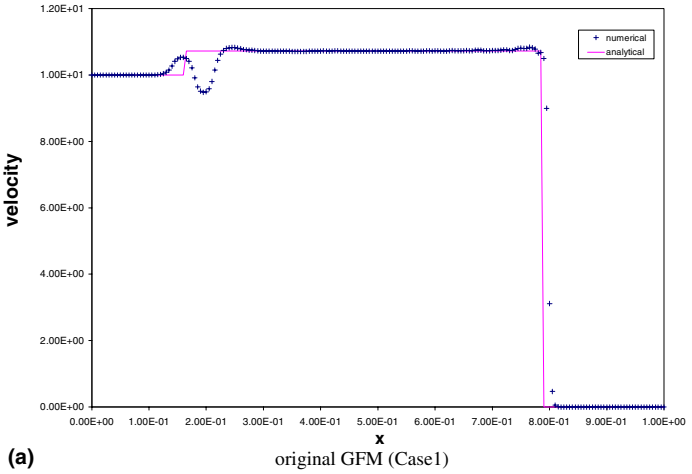

(a) original GFM (Case1)

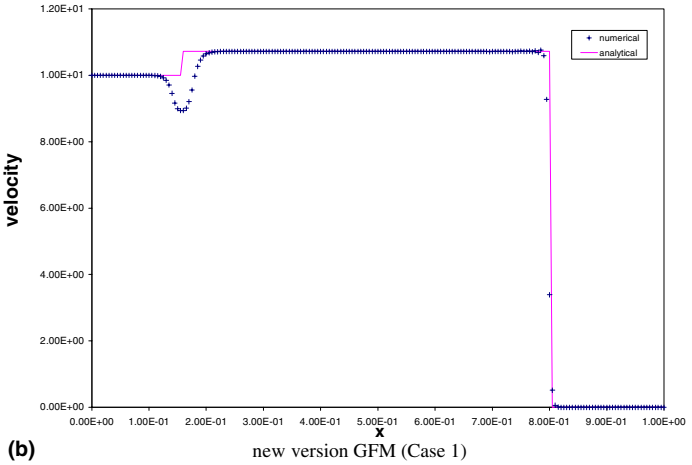

(b) new version GFM (Case 1)

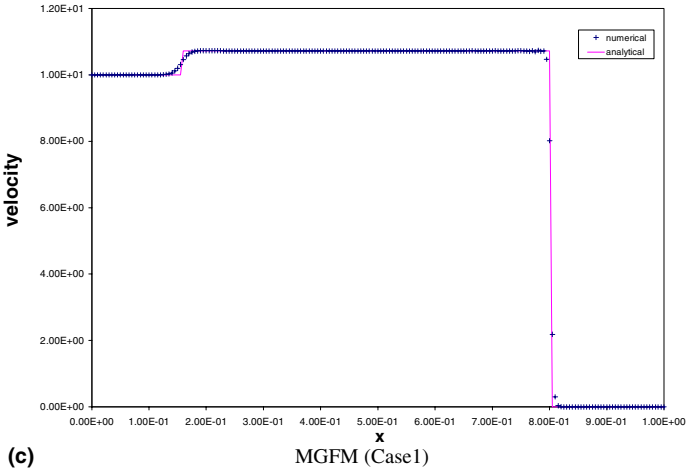

(c) MGFM (Case1)

Fig. 1. Velocity profile for Case 1.

lapsed and no meaningful result is obtained. For the new version GFM, Condition (II) is violated due to the large difference between u_l and u_r. The results by the new version GFM and the MGFM are shown in the respective Figs. 2(a) and (b) for pressure. Severe inaccuracy is incurred by the new version GFM. The MGFM provides a solution comparable to the analysis.

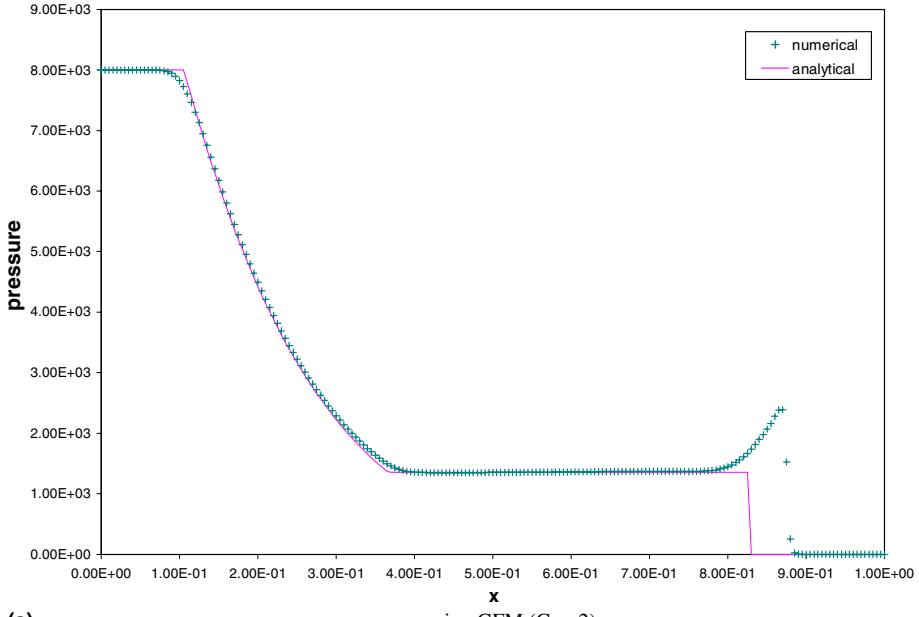

(a) new version GFM (Case2)

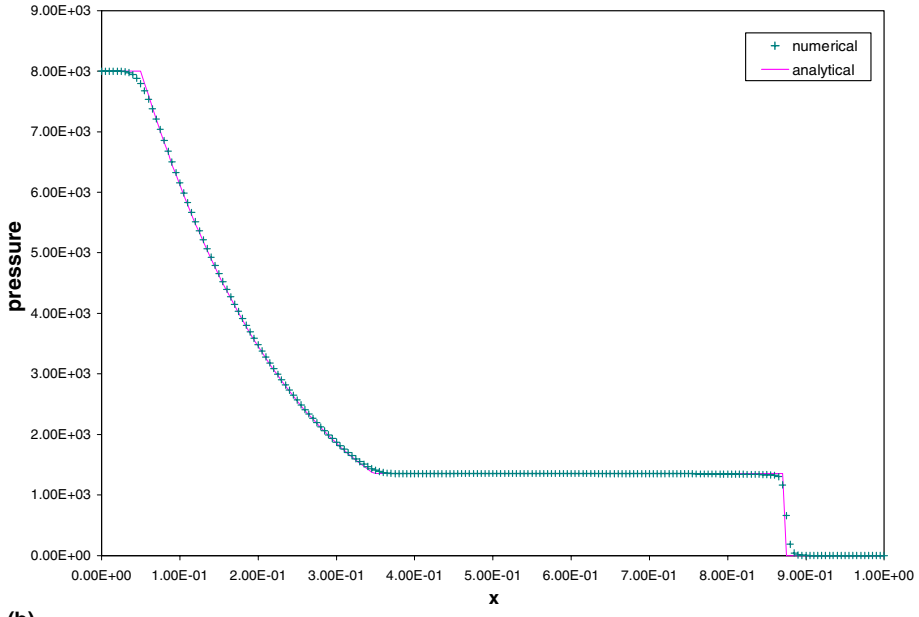

(b) MGFM (Case 2)

Fig. 2. Pressure profile for Case 2.

Case 3. This is a problem of solution type $\overset{G}{S}|\overset{W}{R}$. The initial conditions are $u_l = 100.0$, $p_l = 1.0$, $\rho_l = 0.001$ and $u_r = 0.0$, $p_r = 200.0$, $\rho_r = 1.009$. Condition (I) is violated by the original GFM. The original MUSCL based GFM is unable to provide meaningful results due to severe oscillations incurred (not shown). For the new version GFM, Condition (II) is violated. The pressure plot obtained by the new GFM is shown in Fig. 3(a) with a large discrepancy from the analytical solution. The correct result is provided by the MGFM as shown in Fig. 3(b).

Case 4. This is a problem of solution type $\overset{G}{S}|\overset{W}{S}$. The initial conditions are $u_l = 80.0$, $p_l = 1.0$, $\rho_l = 0.001$ and $u_r = 0.0$, $p_r = 1.0$, $\rho_r = 1.0$. Condition (II) is violated by the original GFM due to the large differ-

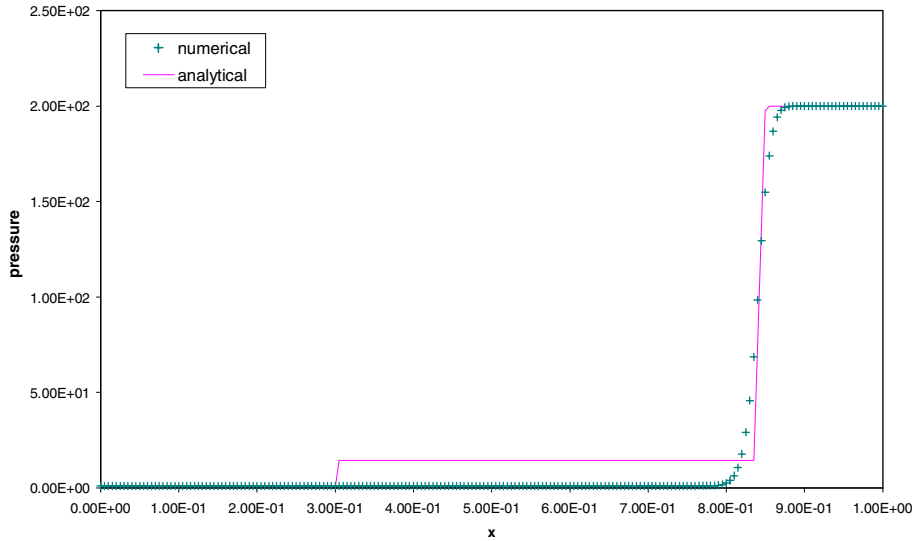

(a) new version GFM (Case3)

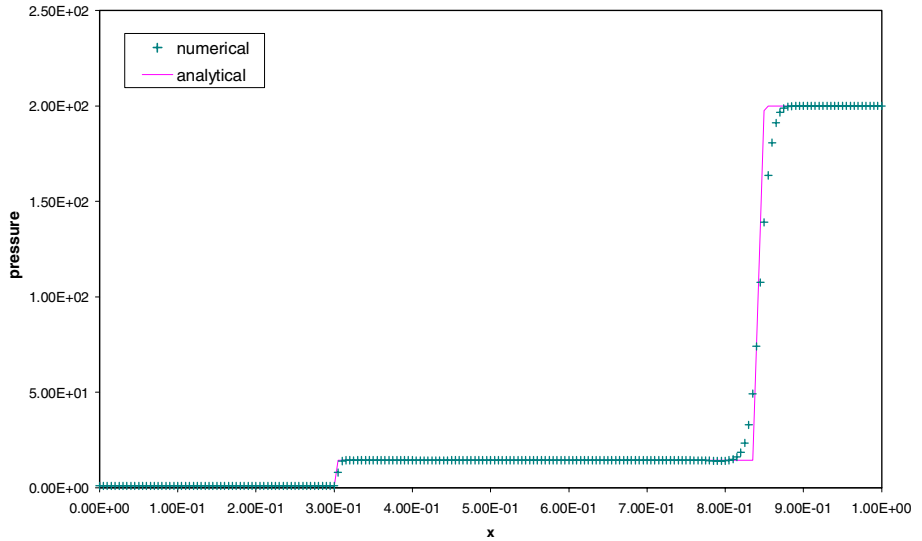

(b) MGFM (Case 3)

Fig. 3. Pressure profile for Case 3.

ence between the initial gas density and the water density. Condition (I) is violated by the new version GFM because of $u_l - u_r > 0$ and $p_l = p_r$. The MUSCL-based original GFM is unable to provide meaningful results due to severe oscillations. The result provided by the new version GFM in Fig. 4(a) is unacceptable, especially for the water region. The result by the MGFM is shown in Fig. 4(b). It is observed, however, that there are some small but limited oscillations behind the transmitted shock using the MGFM. The overall trend and location of the shock front in the water region are not much affected.

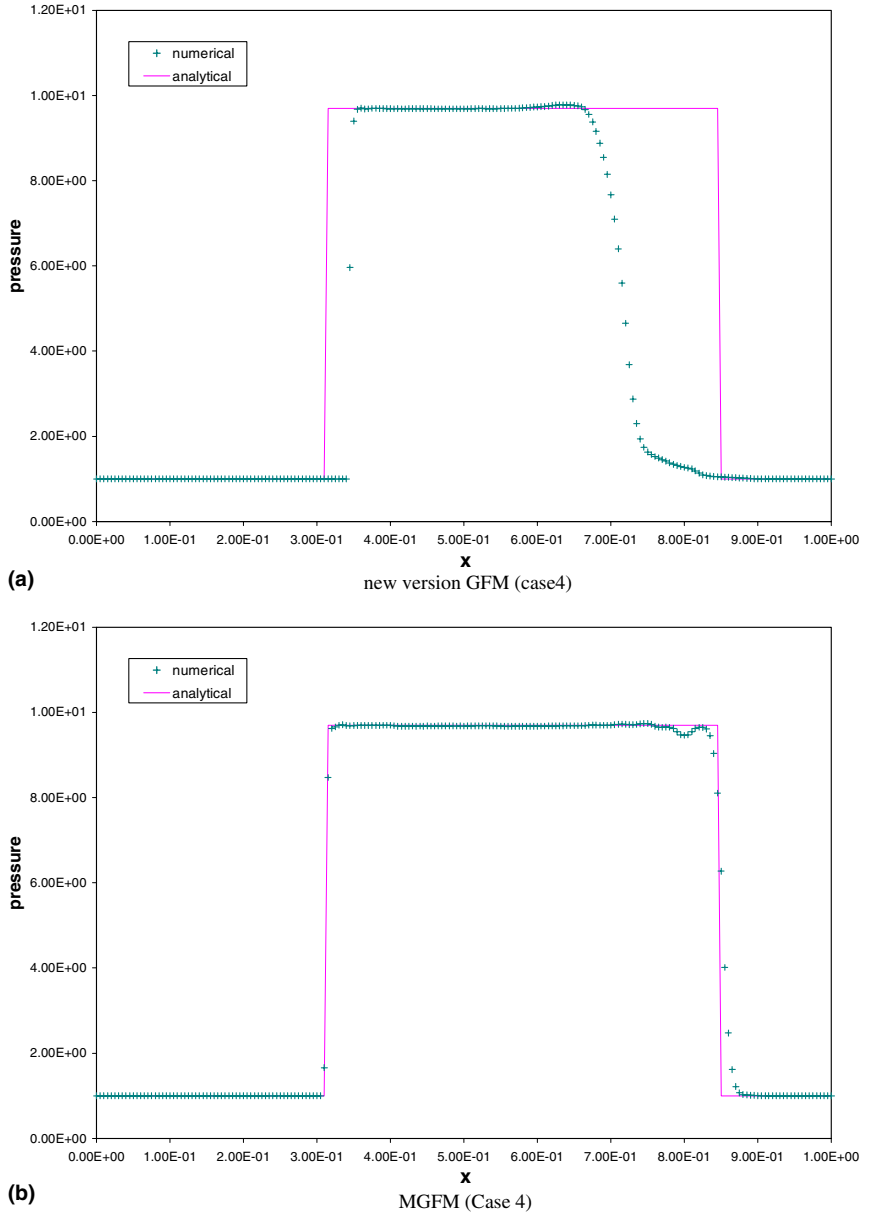

Fig. 4. Pressure profile for Case 4.

Case 5. This is a problem of solution type $\mathrm{R}^{\mathrm{G}}_{\mathrm{R}}|^{\mathrm{W}}_{\mathrm{R}}$. The initial conditions are $u_{\mathrm{l}} = -100.0$, $p_{\mathrm{l}} = 100.0$, $\rho_{\mathrm{l}} = 0.01$ and $u_{\mathrm{r}} = 0.0$, $p_{\mathrm{r}} = 50.0$, $\rho_{\mathrm{r}} = 1.002$. Condition (II) is violated by the original GFM due to the initial gas density being far smaller than the water density. Condition (I) is violated by the new version GFM because of $u_{\mathrm{l}} - u_r < 0$ and $p_{\mathrm{l}} > p_{\mathrm{r}}$. The MUSCL-based original GFM is again unable to provide any meaningful result for this problem. The new version GFM provides a large pressure overshoot in the water shown in Fig. 5(a). The reasonably correct result is obtained by the MGFM with the further modification as discussed in Section 3.4 and shown in Fig. 5(b).

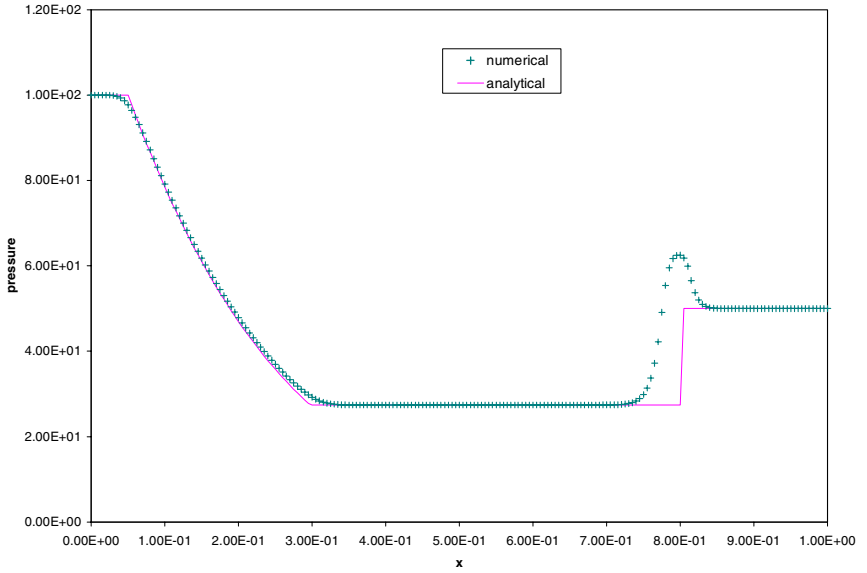

(a) new version GFM (Case5)

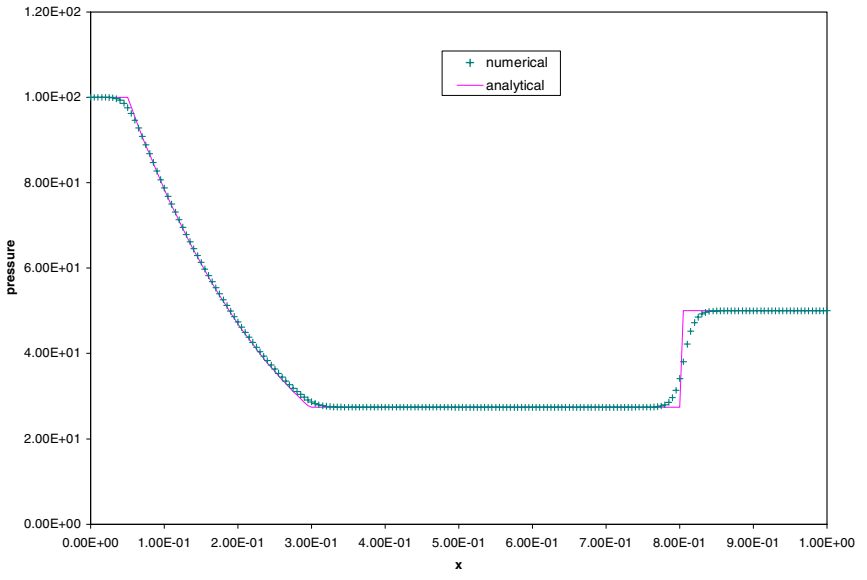

(b) MGFM (Case 5)

Fig. 5. Pressure profile for Case 5.

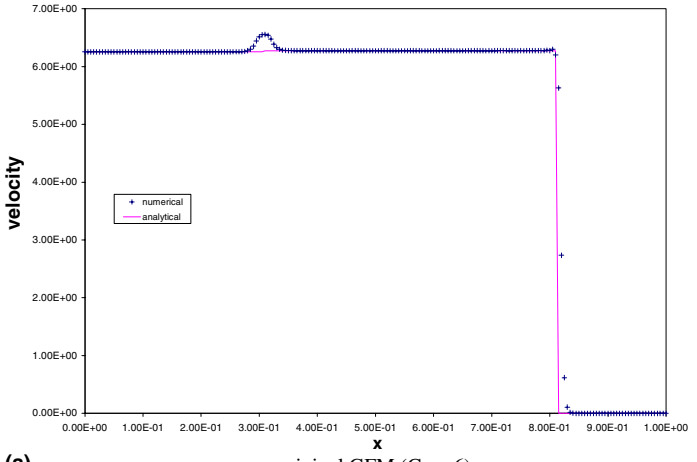

(a) original GFM (Case 6)

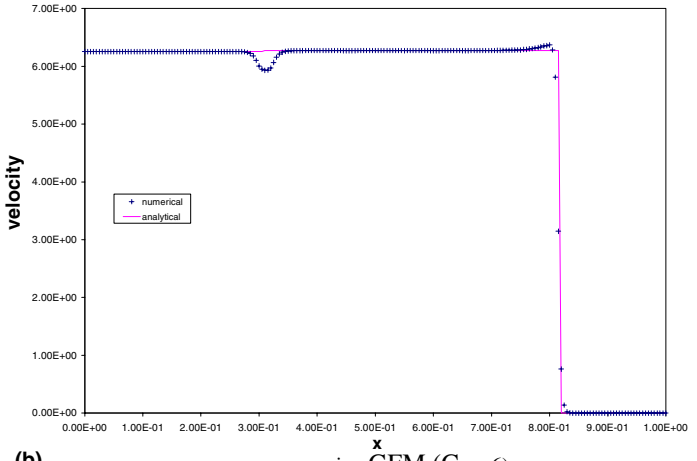

(b) new version GFM (Case 6)

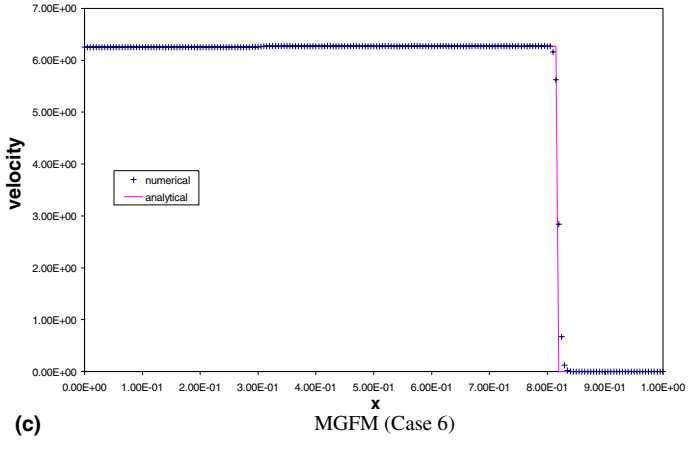

(c) MGFM (Case 6)

Fig. 6. Velocity profile for Case 6.

Case 6. This is a case of the solution type $\overset{\mathrm{G}}{-}\big|\overset{\mathrm{W}}{\mathrm{S}}$. The initial conditions are $u_l = 6.2534$, $p_l = 1000.0$, $\rho_l = 0.8$ and $u_r = 0.0$, $p_r = 1.0$, $\rho_r = 1.0$. The velocity profile by the original GFM is shown in Fig. 6(a) with a distinctly visible hump. The result by the new version GFM is shown in Fig. 6(b) with a trough. The result by the MGFM (Fig. 6(c)) looks reasonable although on much closer scrutiny, there is a very tiny hump in the velocity profile at about the same location as for the original and new GFMs.

Case 7. This is a case of the solution type $\overset{\mathrm{G}}{\mathrm{R}}\big|\overset{\mathrm{W}}{-}$. The initial conditions are $u_l = 0.0$, $p_l = 1000.0$, $\rho_l = 0.8$ and $u_r = 58.6319$, $p_r = 100.0$, $\rho_r = 1.00455$. The MUSCL-based original GFM does not work for this problem. The pressure profile by the new version GFM is shown in Fig. 7(a) with a very large hump.

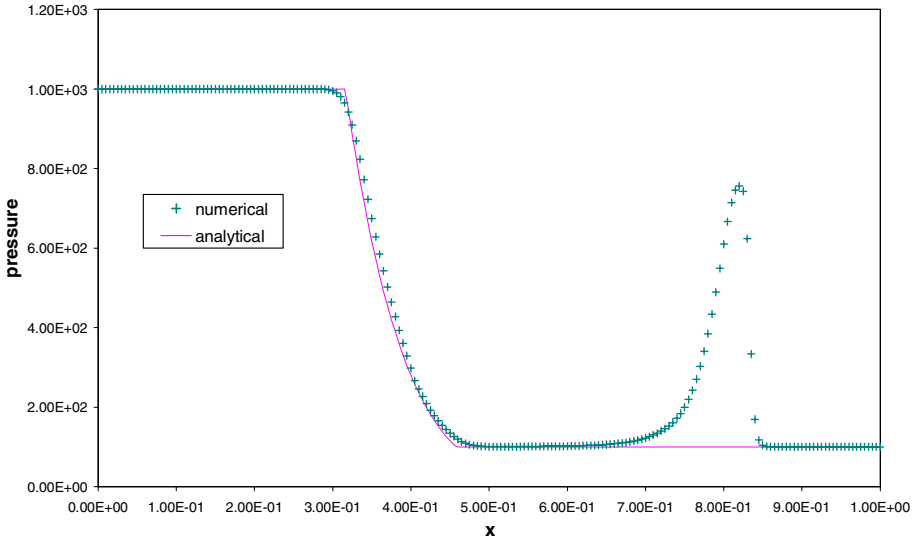

(a) new version GFM (Case7)

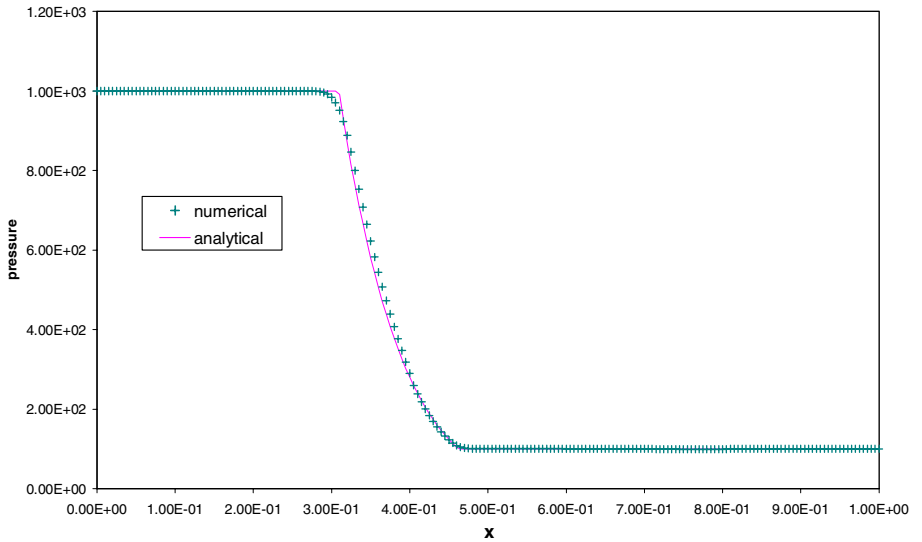

(b) MGFM (Case 7)

Fig. 7. Pressure profile for Case 7.

The result by the MGFM in Fig. 7(b) appears reasonably with a hardly observable trough in the pressure distribution.

Case 8. This is a case of the solution type $\begin{smallmatrix} G \\ S \end{smallmatrix}\Big|_{-}^{W}$. The initial conditions are $u_l = 0.0$, $p_l = 1.0$, $\rho_l = 0.001$ and $u_r = -285.55$, $p_r = 100.0$, $\rho_r = 1.00455$. The MUSCL-based original GFM does not provide any meaningful results for this problem; this is partly attributed to the gas density being very different from the water density. The result by the new version GFM has a large trough and an apparent discrepancy of the shock location in the pressure plot as shown in Fig. 8(a). The result by the MGFM is shown in Fig. 8(b) with only a minor trough in the pressure distribution.

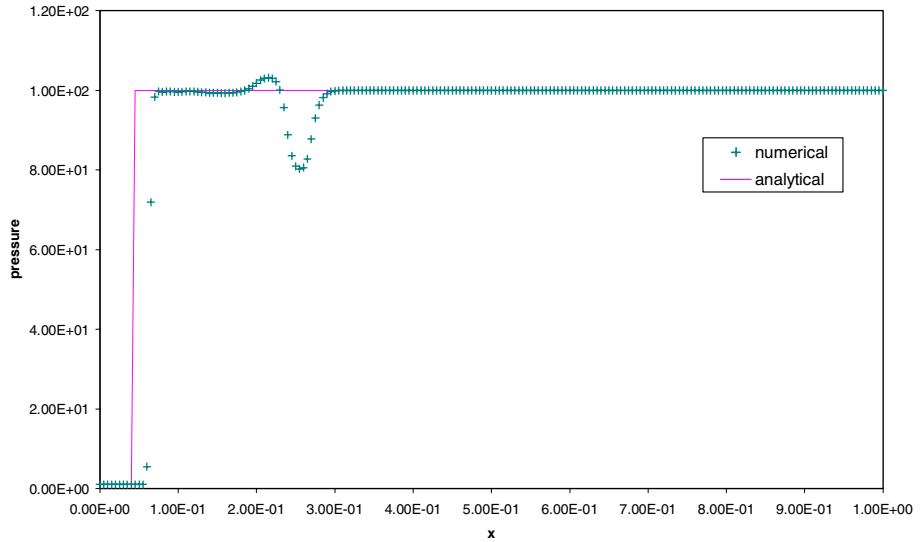

(a) new version GFM (Case8)

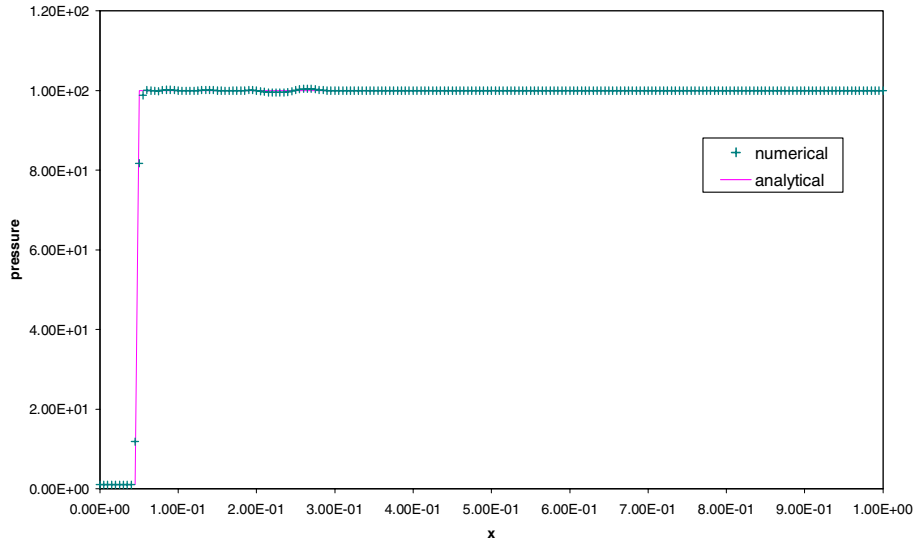

(b) MGFM (Case 8)

Fig. 8. Pressure profile for Case 8.

Case 9. This is a case of the solution type $\frac{\mathrm{G}}{-}|_{\mathrm{R}}^{\mathrm{W}}$. The initial conditions are $u_{\mathrm{l}} = -6.267$, $p_{\mathrm{l}} = 1.0$, $\rho_{\mathrm{l}} = 0.001$ and $u_{\mathrm{r}} = 0.0$, $p_{\mathrm{r}} = 1000.0$, $\rho_r = 1.041$. The MUSCL-based original GFM is unable to generate meaningful results for this problem due partly to the initial gas density being very far smaller than the water density. The result by the new version GFM has an obvious hump in the velocity distribution as shown in Fig. 9(a). The MGFM provides a reasonably correct velocity profile with a barely perceptible hump as shown in Fig. 9(b).

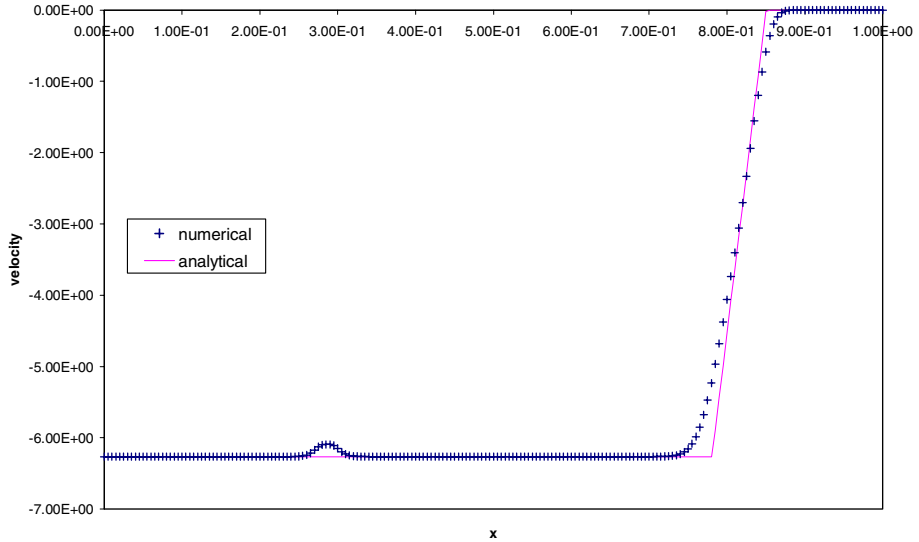

(a) new version GFM (Case9)

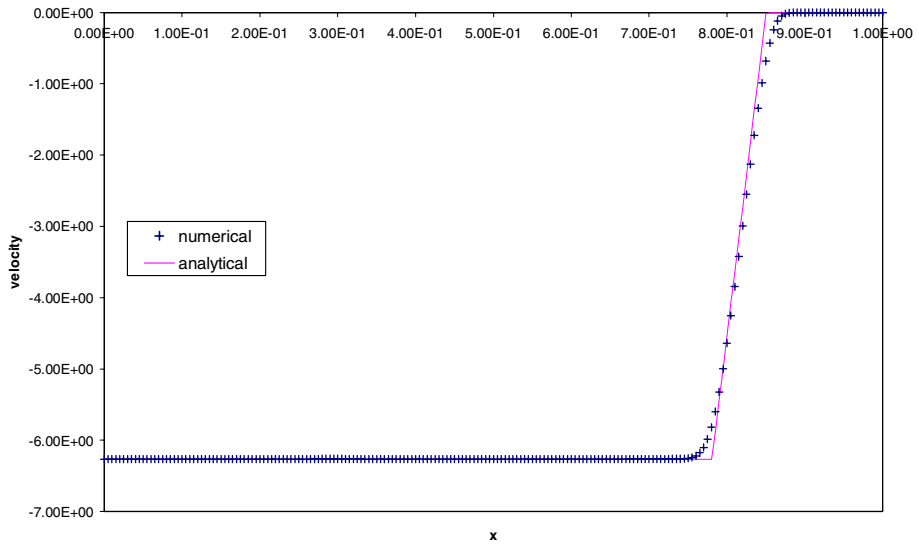

(b) MGFM (Case 9)

Fig. 9. Velocity profile for Case 9.

5. Conclusions

In this work, a systematic analysis and discussion have been carried out for the ghost fluid method (GFM) based algorithm as applied to the gas–water Riemann problems, which was split into two GFM Riemann problems. It has been found that the inability of these two GFM Riemann problems to provide correct and consistent Riemann waves in the respective real fluids may result in inaccurate numerical results. This has led to the suggestion and imposition of Conditions (I) and (II) on the ghost fluid status. The implementation of these two conditions was found to depend on how the ghost fluid status is defined. Using these two conditions, detailed analysis has been carried out for the original GFM [12], the new version GFM [5,13] and the MGFM [20]. It is found that there is a range of conditions for each type of solution where the original GFM and the new version GFM are inherently unable to provide the correct Riemann waves. Moreover, both the original GFM and the new version GFM suffer from obvious numerical inaccuracy when applied to the four special types of solution. Various gas–water Riemann problems, where either the original GFM or the new version GFM or both are unable to provide accurate results, have been constructed to support the present analysis. Numerical tests have also shown that the MGFM with a further modification applied to nearly cavitating flows can provide relatively reasonable results for all the challenging problems presented in this work.

References

[1] R. Abgrall, How to prevent pressure oscillations in multicomponent flow calculations: a quasi-conservative approach, J. Comput. Phys. 125 (1996) 150–160.
[2] R. Abgrall, S. Karni, Computations of compressible multifluids, J. Comput. Phys. 169 (2001) 594–623.
[3] T.D. Aslam, A level set algorithm for tracking discontinuities in hyperbolic conservation laws I: scalar equations, J. Comput. Phys. 167 (2001) 413–438.
[4] T.D. Aslam, A level set algorithm for tracking discontinuities in hyperbolic conservation laws II: systems of equations, J. Sci. Comput. 19 (2003) 37–62.
[5] R. Caiden, R.P. Fedkiw, C. Anderson, A numerical method for two-phase flow consisting of separate compressible and incompressible regions, J. Comput. Phys. 166 (2001) 1–27.
[6] T.-J. Chen, C.H. Cooke, On the Riemann problem for liquid or gas–liquid media, Int. J. Numer. Meth. Fluids 18 (1994) 529–541.
[7] J.-P. Cocchi, R. Saurel, A Riemann problem based method for the resolution of compressible multimaterial flows, J. Comput. Phys. 137 (1997) 265–298.
[8] B. Einfeldt, C.D. Munz, P.L. Roe, B. Sjogreen, On Godunov-type methods near low densities, J. Comput. Phys. 92 (1991) 273–295.
[9] I.I. Glass, J.P. Sislian, Nonstationary Flow and Shock Waves, Oxford Science, 1994.
[10] J. Glimm, L. Xia, Y. Liu, N. Zhao, Conservative front tracking and level set algorithms, PNAS 98 (2001) 14198–14201.
[11] R.P. Fedkiw, A. Marquina, B. Merriman, An isobaric fix for the overheating problem in multimaterial compressible flows, J. Comput. Phys. 148 (1999) 545–578.
[12] R.P. Fedkiw, T. Aslam, B. Merriman, S. Osher, A non-oscillatory Eulerian approach to interfaces in multimaterial flows (the Ghost Fluid Method), J. Comput. Phys. 152 (1999) 457–492.
[13] R.P. Fedkiw, Coupling an Eulerian fluid calculation to a Lagrangian solid calculation with the ghost fluid method, J. Comput. Phys. 175 (2002) 200–224.
[14] P. Jenny, B. Muller, H. Thomann, Correction of conservative Euler solvers for gas mixtures, J. Comput. Phys. 132 (1997) 91–107.
[15] S. Karni, Multi-component flow calculations by a consistent primitive algorithm, J. Comput. Phys. 112 (1994) 31–43.
[16] B. Koren, M.R. Lewis, E.H. van Brummelen, B. van Leer, Riemann-problem and level-set approaches for homentropic two-fluid flow computations, J. Comput. Phys. 181 (2002) 654–674.
[17] B. Larrouturou, How to preserve the mass fractions positivity when computing compressible multi-component flow, J. Comput. Phys. 95 (1991) 31–43.
[18] T.G. Liu, B.C. Khoo, K.S. Yeo, The simulation of compressible multi-medium flow. Part I: a new methodology with applications to1D gas–gas and gas–water cases, Comp. Fluids 30 (3) (2001) 291–314.
[19] T.G. Liu, B.C. Khoo, K.S. Yeo, The simulation of compressible multi-medium flow. Part II: applications to2D underwater shock refraction, Comp. Fluids 30 (3) (2001) 315–337.

[20] T.G. Liu, B.C. Khoo, K.S. Yeo, Ghost fluid method for strong shock impacting on material interface, J. Comput. Phys. 190 (2003) 651–681.
[21] D.Q. Nguyen, F. Gibou, R. Fedkiw, A fully conservative ghost fluid method and stiff detonation waves, in: The 12th International Detonation Symposium, San Diego, CA, 2002.
[22] H.S. Tang, D. Huang, A second-order accurate capturing scheme for 1D inviscid flows of gas and water with vacuum zones, J. Comput. Phys. 128 (1996) 301–318.
[23] E.F. Toro, Riemann Solvers and Numerical Methods for Fluid Dynamics: A Practical Introduction, Springer, New York, 1997.
[24] E.H. van Brummelen, B. Koren, A pressure-invariant conservative Godunov-type method for barotropic two-fluid flows, J. Comput. Phys. 185 (2003) 289–308.